Numerical investigation of rain droplet impact on offshore wind turbine blades under different rainfall conditions

A parametric study

Verma, Amrit; Giovani Pereira Castro, Saullo; Jiang, Zhiyu; Teuwen, Julie

DOI
10.1016/j.compstruct.2020.112096

Publication date
2020

Document Version
Final published version

Published in
Composite Structures

Citation (APA)
Verma, A., Giovani Pereira Castro, S., Jiang, Z., & Teuwen, J. (2020). Numerical investigation of rain droplet impact on offshore wind turbine blades under different rainfall conditions: A parametric study. *Composite Structures*, *241*, Article 112096. https://doi.org/10.1016/j.compstruct.2020.112096

Composite Structures 241 (2020) 112096

Contents lists available at ScienceDirect

Composite Structures

journal homepage: www.elsevier.com/locate/compstruct

Numerical investigation of rain droplet impact on offshore wind turbine blades under different rainfall conditions: A parametric study

Amrit Shankar Verma[a,*], Saullo G.P. Castro[b], Zhiyu Jiang[c], Julie J.E. Teuwen[a]

[a] Faculty of Aerospace Engineering, Aerospace Manufacturing Technologies, Delft University of Technology (TU Delft), Delft 2629 HS, Netherlands
[b] Faculty of Aerospace Engineering, Aerospace Structures and Computational Mechanics, TU Delft, Delft 2629 HS, Netherlands
[c] Department of Engineering Sciences, University of Adger, Grimstad, Norway

ARTICLE INFO

Keywords:
Offshore wind turbine blade
Operation and maintenance
Leading edge erosion
Smooth particle hydrodynamics (SPH)
Coating material

ABSTRACT

The leading edge of a fiber composite wind turbine blade (WTB) is prone to erosion damages due to repeated rain droplet impact during its service life. Such damages are critical to the blade's aerodynamic as well as structural performance, ultimately resulting in substantial repair costs. An effective design of a coating material for WTB is necessary and its analysis must include variables associated with erosive rain droplets such as (1) droplet diameter, (2) impact velocity, and (3) droplet impact angle. The present paper develops and validates a coupled fluid structure interaction (FSI) computational model for simulating rain droplet impact on WTBs, where the structure domain is modelled using conventional finite element method (FEM) and the fluid domain is modelled using smooth particle hydrodynamics (SPH). The 3D numerical model, developed in LS-DYNA, is validated with published experimental results. Further, a parametric study is considered to understand the effects of varying droplet size, impact angles and impact velocities on the impact responses of the leading edge coating system subjected to different rainfall conditions. The rainfall conditions considered for the analysis correspond to four different rainfall intensities (I) – light rainfall (2 mm/hr), moderate rainfall (10 mm/hr), heavy rainfall (25 mm/hr), and very heavy rainfall (50 mm/hr). The results show that the impact responses on the coating system increase with increasing droplet size and increasing droplet impact angle with maximum impulses, stresses and damages developed for normal impingement (90°). Also, the effects of droplet impact angles in the range of 50° to 90° are found critical for rainfall intensities representing very heavy rainfall conditions (I > 25 mm/hr). The results of the peak contact forces and impulses for the above combination of variables used in the numerical study are found in satisfactory agreement with analytical formulations developed through published experiments. Finally, repetitive rain droplet impact analyses are considered and number of impacts required for onset of erosion damages are found to increase by more than seven times upon reducing impact velocities from 140 m/s to 80 m/s for very heavy rainfall conditions (I > 25 mm/hr). The present study is expected to deliver a validated numerical model that can contribute towards enhancing the erosive capacity of a WTB.

1. Introduction

The consistent demand for sustainable sources of power generation has advanced the growth of renewable industry all over the world. Wind turbine technologies, at both offshore and onshore locations, have witnessed a rapid surge in growth in the last decade [1]. Favorable factors such as large open spaces for turbine deployment, seclusion from human settlement, steadier wind conditions and ease in

Abbreviations: FEM, Finite Element Method; SPH, Smooth Particle Hydrodynamics; CFD, Computational Fluid Dynamics; DNV-GL, Det Norske Veritas - Germanischer Lloyd; FSI, Fluid Structure Interaction; OWT, Offshore Wind Turbine; LCOE, Levelised Cost of Energy; MW, Megawatt; UV, Ultraviolet; AEP, Annual Energy Production; 3M, Minnesota Mining and Manufacturing company; PBT, Polybutylende Terephthalate; CEL, Coupled Eulerian and Lagrangian; DEM, Discrete Element Method; SUPG, Streamline-Upwind/Petrov-Galerkin; PSPG, Pressure-Stabilizing/Petrov-Galerkin; CT, Computed Tomography; CZM, Cohesive Zone Method; EOS, Equation of State; ELFORM, Element Formulation type in LS-DYNA code; PDF, Probability Density Function; CDF, Cumulative Distribution Function; ASTM, American Society for Testing and Materials; CSM, Chopping Strand Mat; 3D, Three-dimensional; RSM, Response Surface Method; GFRP, Glass Fiber Reinforced Plastic; RMSE, Root Mean Square Error

* Corresponding author.
E-mail addresses: a.s.verma@tudelft.nl (A.S. Verma), S.G.P.Castro@tudelft.nl (S.G.P. Castro), zhiyu.jiang@uia.no (Z. Jiang), J.J.E.Teuwen@tudelft.nl (J.J.E. Teuwen).

https://doi.org/10.1016/j.compstruct.2020.112096
Received 6 August 2019; Received in revised form 12 January 2020; Accepted 20 February 2020
Available online 26 February 2020

Nomenclature

ρ	Material density (kg/m^3)
V_{tg}	Terminal velocity of rain drop (m/s)
ϕ_d	Droplet diameter (mm)
I	Rainfall intensity (mm/hr)
V_{blade}	Blade tip speed (m/s)
V_{imp}	Impact velocity (m/s)
α	Droplet impact angle (degree)
$\bar{\nu}$	Poisson's ratio
E	Young's modulus of material (MPa)
σ_y	Yield strength of a material (MPa)
σ_y^t	Tensile yield strength of a material (MPa)
σ_y^c	Compressive yield strength of a material (MPa)
ν_s	Dynamic viscosity coefficient (Pa.s)
G	Shear modulus of a material (MPa)
v_s	Velocity of shock wave
v_p	Velocity of particle
C	EOS parameter speed of sound in material (m/s)
γ_o	EOS parameter representing Gruneisen coefficient
a	EOS parameter representing first order correction to
$S1$	EOS parameter representing coefficients of slope of $v_s - v_p$ curve
$S2$	EOS parameter representing coefficients of slope of $v_s - v_p$ curve
$S3$	EOS parameter representing coefficients of slope of $v_s - v_p$ curve
k	Contact stiffness
$SOFSCL$	scaling factor for constraint forces
m	Nodal mass
Δt	Step size
$A(x_i)$	Arbitrary property of each particle
h	Smoothing length
W	Interpolation function
$F_x(\phi_d)$	Cumulative Distribution Function of droplet diameter
σ_n	Normal stresses at the interfaces
σ_s	Shear stresses at the interfaces
$NFLS$	Interlaminar normal strength
$SFLS$	Interlaminar Shear strength
E_{11}	Longitudinal modulus of composite
E_{22}	Transverse modulus of composite
E_{33}	Transverse modulus of composite
G_{12}	Inplane shear modulus of composite
G_{13}, G_{23}	Out of plane shear modulus of composite
X_T	Tensile strength of composite in the principal fibre direction
X_C	Compressive strength of composite in the principal fibre direction
Y_T	Tensile strength of composite in the transverse fiber direction
Y_C	Compressive strength of composite in the transverse fiber direction
Z_T	Tensile strength of composite in through-the-thickness direction
Z_C	Compressive strength of composite in through-the-thickness direction
S_{12}	Inplane shear strength of composite
S_{13}, S_{23}	Out of plane shear strength of composite

transportation of offshore wind turbine (OWT) components on barges, have made offshore wind extremely popular and competitive with onshore wind industry [2]. However, one of the main challenges is the relatively high operation and maintenance costs associated with OWTs, which increases the net Levelised Cost of Energy (LCOE). One of the ways to tackle this cost issue is to deploy turbines with high power ratings, thereby reducing the number of turbines at an offshore farm for a given power capacity [3]. Fig. 1(a) presents the demand in the power ratings of OWTs over several years, where it can be clearly seen that power ratings of turbines greater than 5 MW-8 MW are currently in high demand. Such turbines are efficient in increasing the power output, however, one of their main issues is the increase in size of their components posing several engineering challenges [4]. For instance, large size blades of lengths more than 80–100 m are being developed, and these blades must be designed such that they are able to withstand severe stresses and strains developed due to complex loading cycles during operations. Another major challenge is related to the material degradation of the wind turbine blade during its service life due to environmental factors such as exposure to ultraviolet (UV) action and precipitations in the form of rain and hail [7,8].

The leading edge of a fiber composite wind turbine blade is prone to erosion damages (Figs. 2(a)-(b)) due to repeated rain droplet impact during its service life [9,10]. Such damages are critical to the blade's structural and aerodynamic requirements, ultimately resulting in substantial repair costs. It has been found in [11] that the erosion and contamination of leading edges can cause an increase of about 314% in the drag coefficient and corresponding reduction of 53% in the lift coefficient, thereby being a critical factor to the annual energy production (AEP) of a turbine. Further, due to the increasing blade length and related high tip velocity in modern wind turbine blade designs, the issue of leading edge erosion becomes more critical [12]. For instance, Fig. 1(b) shows how the tip speed of a wind turbine blade varies for

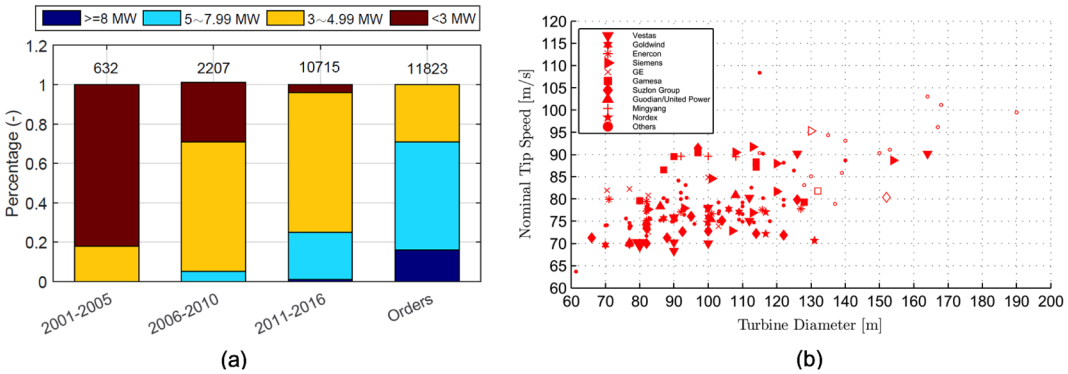

Fig. 1. (a) Offshore wind turbine size demand based on commercial orders since 2001 [5] (b) Blade tip speed based on rotor diameters for different commercial blades [6].

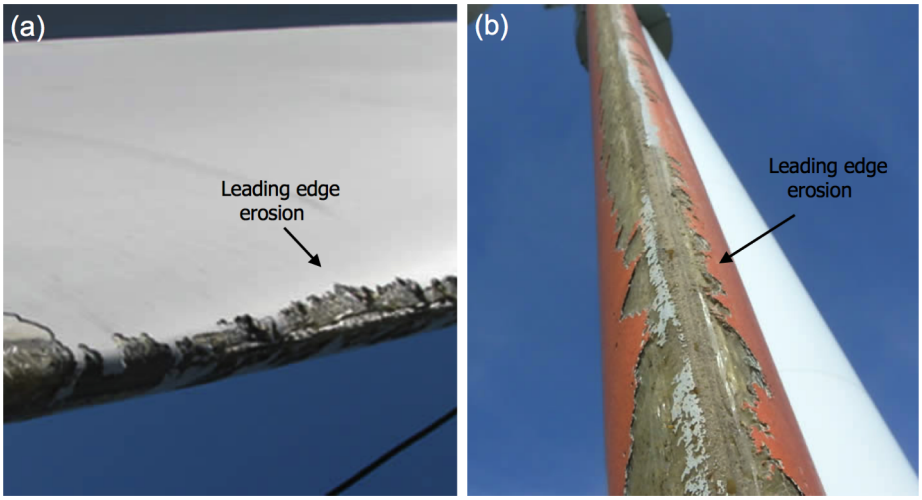

Fig. 2. Leading edge erosion of wind turbine blades [16].

different rotor diameters. The tip speed of the blades can range between 70 and 110 m/s for existing turbines, and their impact with the rain droplet at high velocities can induce large stresses on the leading edge. In addition, the damage mechanisms for the leading edge erosion are complex and consist of simultaneously interacting multiple failure modes such as material fatigue, local pitting, fatigue cracks in coatings and composites, delamination and roughening of surfaces [13–15].

Given that the leading edge erosion directly affects the power output of a wind turbine and has a high economic influence, the OWT industry is seeking effective solutions to prevent erosion of wind turbine blades. Different coating materials such as those based on multilayered flexible polyurethane coating systems are being developed and tested in erosion testing machines [4,10,17]. 3M [18] provides polyurethane based elastomeric protection tapes that can be added to the blade after manufacturing with the intent of providing good erosive capacity against rain as well as sand and debris [18]. However, it is to be noted that such tapes are prone to interfacial delamination if there is insufficient adhesion between coating and laminate, thereby requiring frequent replacement [12]. A primer layer was recommended between the coating and laminate [19], which significantly improved the delamination resistance at the interface. Slot et al., [10] tested injection molded and compression molded polybutylende terephthalate (PBT) material against rain erosion testing. The authors found PBT based thermoplastic coating as an effective alternative against polyurethane coatings. PBT based thermoplastic coating does not add significant weight to the blade and exhibits high rain erosive resistance. Armor Edge [16] produces tough thermoplastic semi-flexible leading edge protection shields, which are used in the industry for repairing leading edge erosion. Another industrial solution emphasises on control engineering perspective where the idea is to reduce the impact velocity between the rain droplet and leading edges during operational phases. Five different control strategies have been proposed in [20] for reducing the tip speed of the blade during harsh precipitations, thus preventing large impact pressures on the coating material due to rain droplet impact. In this way, the stresses are expected to be maintained well below the endurance limit of the coating material, thereby inhibiting fatigue damage accumulation [9,21].

In addition to these solutions, it is also essential to develop computational models to simulate rain erosion of wind turbine blades. Such models would contribute towards identifying the key failure mechanisms behind the rain erosion, design and optimise the coating materials at the leading edge against the rain-induced wear, along with estimation of fatigue life of the coating material [21]. Furthermore, validated computational models can be used to evaluate the erosive strength of all the aforementioned materials at significantly reduced costs when compared to experimental tests for the same purpose. Keegan et al. [22] used the coupled Eulerian and Lagrangian (CEL) method to model rain droplet impact on wind turbine coating materials. An epoxy based gelcoat material was considered, together with droplet diameter of 3 mm and impact velocity ranging till 140 m/s. The impact pressure obtained by the authors closely correlated with the analytical water hammer pressure. Keegan et al. [12] also utilised the smooth particle hydrodynamics (SPH) method to simulate rain and hail impact on wind turbine coating material, and the method correlated well with the experiments. The SPH method for rain droplet impact has also been investigated by Astrid et al. [23] where coatings were modelled using conventional Finite Element methods (FEM) methods. The study showed that the SPH formulations are limited in capturing the independent motion of rain droplet impacting the blade. An alternative Discrete Element method (DEM), also based on meshless formulations, was recommended to model rain droplet impact. Corsini et al. [24] utilised a Streamline-Upwind/Petrov-Galerkin (SUPG) and Pressure-Stabilizing/Petrov-Galerkin (PSPG) stablisation method together with particle-cloud tracking approach and estimated the key regions along the blade that are critical for erosion. In another work, Corsini et al. [25] analysed rain erosion on baseline and an aerodynamically optimised 6 MW wind turbine blade and the Lagrangian method was utilised to model rain droplet flow. It was found that although the blade with optimised aerofoil shape had a good aerodynamic performance, the region of maximum erosion shifted from the blade tip to the middle region of the leading edge. Therefore, it was recommended that optimisation process of aerofoil should consider rain erosive aspect together with target of enhanced aerodynamic performance. Cortes et al. [17] utilised the cohesive zone approach to model the interfaces between coating and laminate, and investigated the single rain droplet performance of flexible coatings. Fraisse et al. [26] developed a coupled Eulerian-Lagrangian symmetric model to study impact of water droplet on coated laminate of the blade. The coated material was modelled in Eulerian domain whereas water droplet was modelled in Lagrangian domain. CT scan measurements were made at the gelcoat material, and the results correlated well with the findings from numerical simulations. In summary, the computational models for rain erosion make up an important tool in understanding the physical process of erosion together with contributing to design of coating materials against rain erosion.

Most of the computational models developed in the aforementioned literatures do not consider parameters which indicate representative rainfall conditions for rain erosion analysis of a wind turbine blade. It has also been pointed out in [27,28] that an effective design and analysis of a coating material must include variables associated with

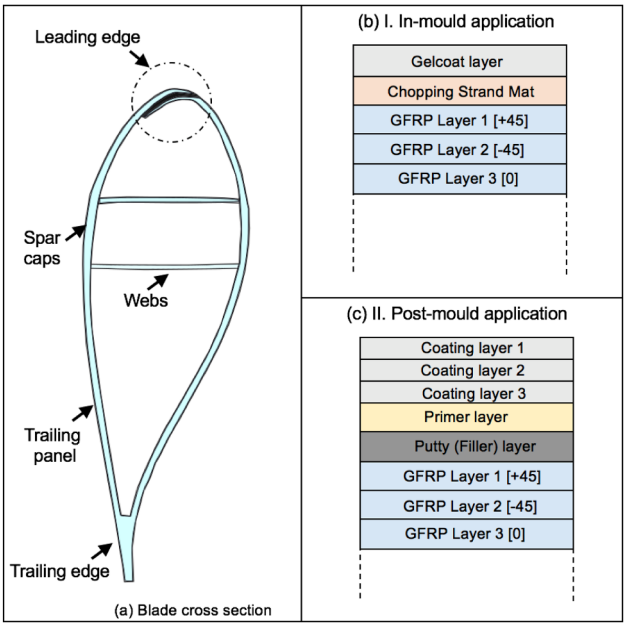

Fig. 3. (a) Typical blade cross section (b) Gelcoat-based in-mould coating (c) Flexible post-mould leading edge coatings applied in different layers together with putty and primer.

erosive rain droplets, such as (1) droplet diameter, (2) impact velocity, and (3) droplet impact angle, and the coating material must exhibit resistance to erosion under different rainfall conditions. Although Amirzadeh et al. [29,30] developed a computational framework considering such aspects for assessing rain erosion in wind turbine blades, a decoupled fluid structure interaction (FSI) problem was considered. Impact pressure on the coating material due to rain droplet impact was obtained using Computational Fluid Dynamics (CFD) simulations, where a stochastic rain texture model was used to simulate rain fields corresponding to different rainfall conditions. Subsequently, the impact pressure obtained from CFD analysis was used in a separate Finite Element Method (FEM) study to estimate the fatigue life of a wind turbine blade. Modelling of rain droplet impact using such conventional Eulerian-based CFD solvers is computationally demanding and requires a large CFD mesh comprising all regions reachable by the water flow, with enough refinement to keep track of the free fluid surface with sufficient accuracy. In this paper, we develop a more efficient computational model where a coupled FSI interaction model for rain droplet impact on a wind turbine blade is developed and validated. The structural domain representing the wind turbine blade is modelled using conventional finite element methods, whereas the fluid domain is modelled using SPH. The developed numerical model allows a direct fluid structure interaction (FSI) coupling by simultaneously solving the displacement evolution of the SPH particles' and FE nodes, whereby load transfer between both domains is attained via a penalty contact algorithm explained in the following sections. Further, only the region encompassed by the fluid is modeled with SPH particles such that the free fluid surface evolution is naturally represented by the particles' kinematics. Also, droplet sizes and droplet impact velocities considered for the analysis in this study represent four different rainfall intensities - light rainfall (2 mm/hr), moderate rainfall (10 mm/hr), heavy rainfall (25 mm/hr), and very heavy rainfall (50 mm/hr). Finally, a numerical model for simulating repetitive rain droplet impact on leading edge coating system is considered and number of impacts for onset of erosion damages are compared for different blade tip velocities. All in all, the novelty of the present paper is threefold: (1) a validated coupled FSI computational model for rain droplet impact analysis on a wind turbine blade, (2) computational model considering parametric analysis, where input variables represent different rainfall conditions which a wind turbine blade is expected to face during its service life, and a (3) coupled FSI model for repetitive rain droplet impact analysis, where number of impacts required to initiate erosion 'damages on the coating material are estimated.

The remaining of the paper is organised as follows. Section 2 describes the problem definition and analysis procedure. Section 3 describes the background of SPH method and contact algorithm used in this study for FSI model. Section 4 presents material and modelling method. Section 5 presents the results and discussion. Section 6 concludes the paper. Finally, limitations of the current work as well as recommendations for future studies are described in Section 7.

2. Problem definition and analysis procedure

A wind turbine blade design is an optimisation between the standpoints of aerodynamic requirement and structural strength demand [31]. In their vast majority, wind turbine blades are manufactured using composite laminates consisting of glass or carbon fibers embedded in thermosetting polymeric resins [10]. The composite materials provide high strength and stiffness to weight ratio, while providing high fatigue strength and fracture toughness. However, these material systems are weak in fiber off-axis direction, making them vulnerable to transverse (out of plane) impact loads [32]. Additionally, these materials are sensitive to environmental exposure of moisture, ice, hail, UV and rain, thereby requiring coating materials to be applied on the top surface of the blade to avoid material degradation.

Currently, the blade manufactures use two broad categories of surface coating materials for increasing the life cycle of wind turbine blades. The first category of coating material is based on epoxy or polyester based gelcoat material [17,8] and is applied in-mould during the manufacturing of the wind turbine blades (Fig. 3b). The type of gelcoat material is made compatible with the epoxy resin used for blade infusion, and provides an advantage of efficient integration with the blade system [33]. In addition, the gelcoat materials also provide a smoother blade surface at the leading edges, thus enhancing aerodynamic performance of the blade. According to the DNV-GL guideline [33], gelcoat material is an essential design parameter for blade durability, and must qualify for (a) having sufficient substrate adhesion (2–3 MPa in pull off tests), (b) mechanical strain should exceed the design strain limits of the laminates, (c) resistant properties against UV exposure, and (d) erosion resistant for leading edge applications due to factors such as hail and rain. The guideline recommends that a typical gelcoat thickness for a wind turbine blade should be between 0.3 to 0.6 mm, which is crucial for sound rain erosion resistance.

The second category of coating system involves applying polyurethane based flexible coating or leading edge protection tape [17,34] to the blade post its manufacturing process (Fig. 3(c)). Flexible coating materials are applied in multiple layers together with additional putty or primer layer added between substrate and coating to enhance adhesion. Given that the elastomeric coating materials have low dynamic impedance compared to the substrate, the substrate-coating adhesion is of primary importance. Any delamination or debonding between coating and substrate is expected to accelerate the rain erosion process. In [17] a numerical modelling approach based on cohesive zone methodology (CZM) is implemented to model delamination between substrate and coating. The numerical model also included the primer layer at the coating-adhesion interfaces, and it is expected that such models can be used to optimise the interface material to enhance adhesion. It is recommended [17] that elastomeric coatings must be applied in limited number of layers, as this aids in the reduction in the number of interfaces between coating and substrate. The present paper considers the first category of coating material i.e. gelcoat material for analysis of rain droplet impact on a wind turbine blade. The reason for choosing gelcoat material for the analysis is that they have been widely used in the blade industry for many years and their material properties are well defined in the literature for rain droplet simulations. The

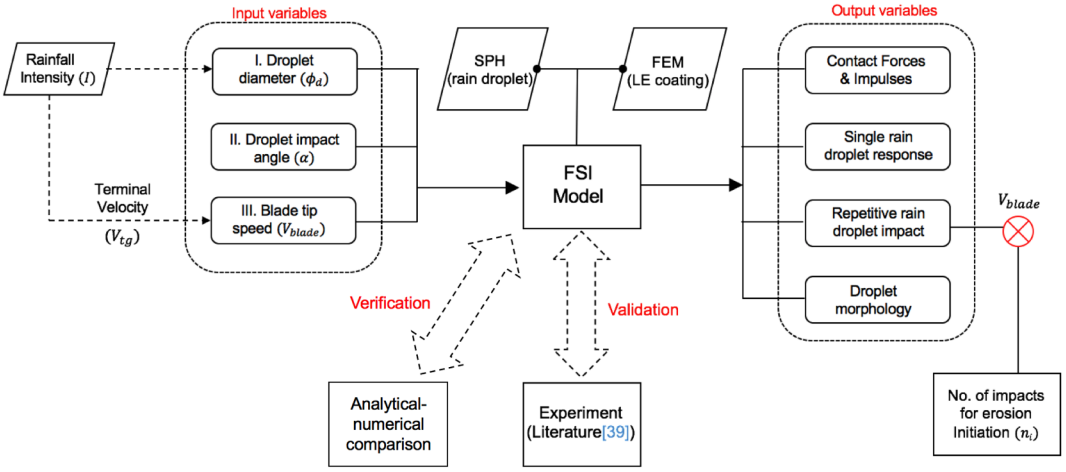

Fig. 4. Analysis procedure considered in the paper.

analysis on flexible polyurethane based coating layer will be considered in future work.

Fig. 4 presents the analysis procedure considered in this paper. First, a coupled fluid structure (FSI) computational model is developed in LS-DYNA numerical code to simulate single rain droplet impact and is validated with published experimental results from the literature. Next, the numerical model is extended to understand the effect of varying droplet size, droplet impact angle and impact velocities on the impact responses of the leading edge coating system subjected to different rainfall conditions. Different rainfall intensities are considered for choice of droplet size and droplet velocity, and important results include the assessment of contact forces, impulse, damages and droplet morphology due to single rain droplet impact. An analytical-numerical verification of these results are also presented. Finally, a repetitive rain droplet impact is considered and number of impacts for initiation of erosion damages are compared for different blade tip velocities. Repetitive rain droplet impact is employed through a script where the damage state of the coating material from one droplet impact is transferred to the next analysis for subsequent droplet impact. In this way, erosion state in the coating system due to accumulated damage is simulated. The details of the input parameters, rainfall conditions, as well as the numerical modelling method will be described in the subsequent section.

3. Description of the SPH method and contact algorithm for FSI model

A brief background of the smooth particle hydrodynamics (SPH) method as well as the details of the contact algorithm used in this study is presented below.

3.1. Background of the SPH method

Smooth particle hydrodynamics (SPH) method is a meshless Lagrangian technique for modelling transient fluid dynamics by utilising pseudo-particle interpolation scheme [35,36]. This method was first introduced in the field of astrophysics [37] where motion of particles in space were simulated. Given that there are no presence of grid in the computational domain, the method is highly efficient in solving non-linear problems associated with significant mesh deformations or distortions. In this method, fluid is defined by a set of moving particles, where individual particle corresponds to an interpolation point with known fluid properties. A kernel function, also described as the interpolation function, is utilised in the formulation which describes the required quantities for all the defined particles. Every single particle defined by the SPH formulation corresponds to a mass and can also represent hydrodynamic (pressure, velocity) and thermodynamic (temperature, phase changes) state of the fluid at that point. The arbitary property $A(x_i)$ of each particle i in the SPH domain is given by the approximated smoothed value ($A^h(x_i)$):

$$A^h(x_i) = \sum_{j=1}^{N} m_j \frac{A(x_j)}{\rho(x_j)} W(x_i - x_j, \tilde{h}) \tag{1}$$

where x_i are the coordinates of the considered particle i, x_j, m_j, $A(x_j)$, and $\rho(x_j)$ are the coordinates, mass, property and the density of the neighboring particle j respectively. $W$is the interpolation (kernel) function, and is related with the smoothing length $h$and the position of the neighboring particle. Note that the summation defined in Eq. (1) is performed over all the particles in the SPH domain, and within a radius of $2h$(Fig. 5(a)). The contribution of the properties of each of the neighboring particles towards the property of a considered particle is governed by the interpolation (kernel) function W. The interpolation function (W) is given by:

$$W(x_i - x_j, \tilde{h}) = \frac{1}{h}\theta\left(\frac{x_i - x_j}{h}\right) \tag{2}$$

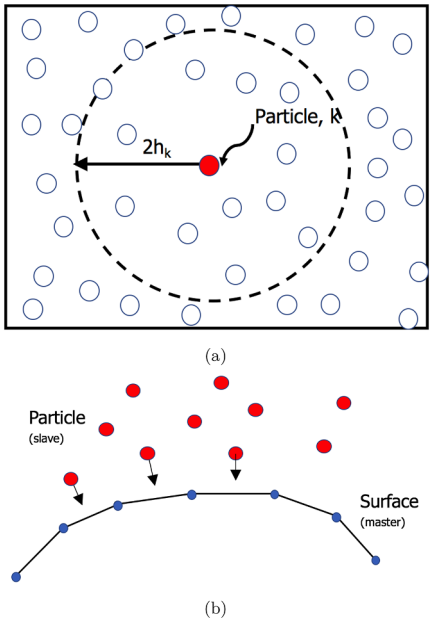

Fig. 5. (a) Active domain for a particle in SPH method (b) particle to surface based contact algorithm.

where θ in the Eq. (2) is the smoothing kernel function, which is defined by the cubic B-spline function as:

$$\theta(v) = c^* \begin{cases} 1 - \frac{3}{2}v^2 + \frac{3}{4}v^3 & v \leq 1 \\ \frac{1}{4}(2-v)^3 & 1 \leqslant v \leqslant 2 \\ 0 & v \geqslant 2 \end{cases} \tag{3}$$

where c is the constant of normalization that is dependent upon space dimensions. The conservation of mass using SPH approximation is given as:

$$\frac{d\rho}{dt}(x_i) = \sum_{j=1}^{N} m_j \frac{\rho}{\rho_j}(v(x_j))\nabla W_{ij} \tag{4}$$

The conservation of momentum using SPH approximation is given as:

$$\frac{dv}{dt}(x_i) = \sum_{j=1}^{N} m_j \left[\frac{P(x_i)}{\rho_i^2}\nabla W_{ij} - \frac{P(x_j)}{\rho_j^2}\nabla W_{ji} \right] \tag{5}$$

3.2. Contact algorithm for fluid structure interaction

One of the essential steps in analysing impact problems using finite element solvers is appropriate modelling of contact interaction between the impactor and the target. In case, the stiffness of the impactor is relatively high compared to the stiffness of the target, the impactor is commonly modelled as rigid given that there will be negligible deformation or change of state of the impactor. In such cases, the contact interaction between target and impactor can be defined based on node to surface or surface to surface contact algorithm. However, in the cases where there is substantial deformation and rapid deceleration of the impactor at the point of impact, such as impact of rain droplet on a material with high velocity, a fluid structure interaction problem is formulated. The rain droplet is modelled in this study using a set of moving particles using SPH method, whereas structure domain is discretised using nodes and elements using traditional FEM methods. The contact interaction is defined between them in this study using particle to surface contact algorithm where the fluid particle is assigned as the slave, and the target structure is defined as the master surface in the formulation (Fig. 5(b)). In course of the calculation, at each time step, perpendicular distance between the slave particle and master solid surface is checked, and in case there is a penetration, a contact interface force is applied. The interface force exerted is equal to the product of contact stiffness (k) and resulting penetration between particle and solid surface and the effect is equivalent to presence of a spring at the interface. The contact spring stiffness (k) is defined using soft constraint based approach (SOFT = 1 in LS-DYNA *CONTACT card) and is given by [38]:

$$k = SOFSCL\frac{m}{\Delta t^2} \tag{6}$$

where $SOFSCL$ is the scaling factor for constraint forces taken as 0.25, m is the nodal mass, Δt is defined as time step size of the simulations and is determined automatically by the LS-DYNA solver. The above discussed soft constraint formulation is recommended in LS-DYNA [38] for cases where impact include dissimilar materials having large difference in stiffness.

Fig. 6 presents the calculation cycle of SPH method utilised in the LS-DYNA numerical code. The computational steps followed are in general similar to the classical FEM, however, certain steps involve use of kernel approximations specific to SPH method discussed before. The steps critical for SPH calculation include the ones marked with red boundaries in Fig. 6 i.e, it consists of (a) estimation of initial smoothing length for defining the domain of interactions among particles, (b) definition of neighbouring particles using a bucket sort algorithm (using the flag INI = 0 in LS-DYNA), (c) estimation of density and strain rates by utilising the spatial derivatives of velocities, and (d) estimation of forces from the spatial derivatives of stresses.

4. Material and modelling method

In this section, the numerical modelling details for the verifications and validation study as well as the rain droplet impact investigation on the leading edge gelcoat system are presented. A coupled FSI computational model is developed in LS-DYNA numerical code where the fluid domain is modelled using smooth particle hydrodynamics (SPH) and structure domain representing wind turbine blade is modelled using conventional Finite Element Method (FEM) method. A particle-to-surface based penalty contact algorithm, as discussed before, is defined between rain droplet and leading edge coating system, enabling the calculation of all necessary internal forces that represent fluid structure interaction.

4.1. Validation study

A validation model representing a coupled FSI formulation is developed using LS-DYNA numerical code and results are compared with experiments performed in [39]. Fig. 7(a) presents the schematics of the test setup used in [39] for studying single water droplet impact on the aluminum plate of dimensions 20 mm × 20 mm × 1 mm. A piezoelectric transducer is attached to the bottom of the plate which measures the contact forces generated due to water droplet impact. It is to be noted that in [39], impact responses of different droplets with varying sizes, shapes and impact speeds were studied. However, in the current study, three spherical droplet sizes of diameter 2.70 mm, 2.90 mm, and 3.54 mm with five different impact velocities (1.36 m/s, 1.92 m/s, 2.32 m/s, 2.67 m/s, 2.99 m/s) are considered for the validation purpose.

Fig. 7(b) presents the developed numerical model with water droplet discretised using SPH particles where a total of 135 k particles are used. The number of particles used in the model is based on a convergence study, where the impact forces obtained from the analysis are checked against the measured values from the experiment. The details of the convergence study will be described in the next section. The water droplet is defined with *MAT NULL material model, together with Equation of State (EOS) based on Gruneisen formulation to include the compressibility. The Gruneisen formulation [38] defines the pressure for a compressible material (P) and relates linearly the shock wave velocity with the particle velocity (also known as v_s-v_p EOS) and is given by:

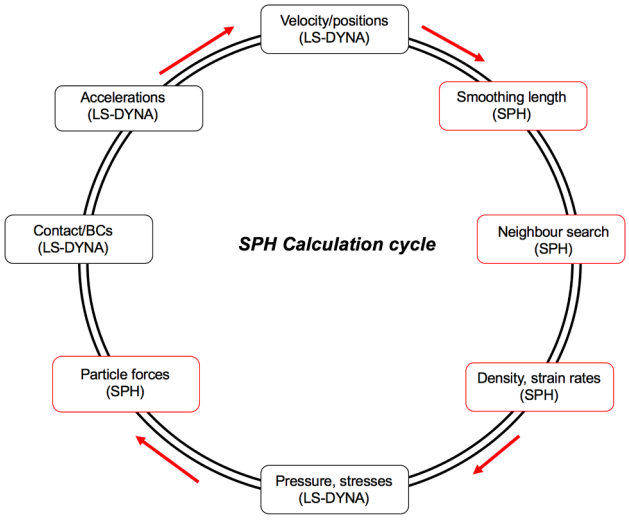

Fig. 6. Calculation cycle of SPH method in LS-DYNA [38].

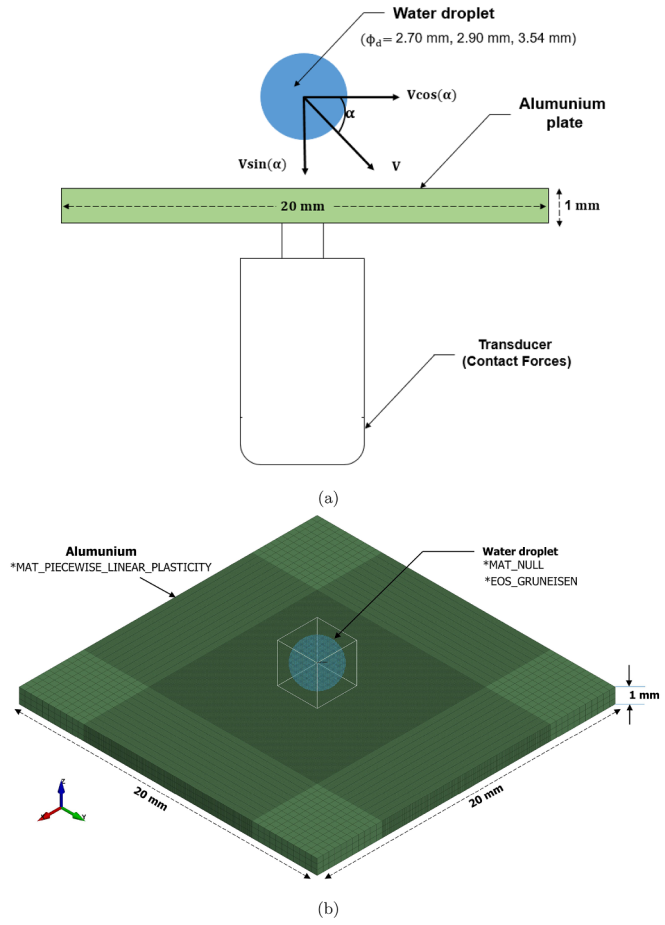

Fig. 7. (a) Schematics of test setup used in [39] (b) Numerical model for validation study.

$$P = \frac{\rho C^2 \mu \left[1 + \left(1 - \frac{\gamma_o}{2}\right)\mu - \frac{a}{2}\mu^2\right]}{1 - (S_1 - 1)\mu - S_2\frac{\mu^2}{\mu+1} - S_3\frac{\mu^3}{(\mu+1)^2}} + (\gamma_o + a\mu)e \tag{7}$$

where C is the Y-intercept of the $v_s - v_p$ curve and represents bulk sound speed, S1, S2 and S3 are the coefficients of the $v_s - v_p$ curve's slope, γ_o refers to Gruneisen coefficient, a is the first order correction to γ_o, ρ is the material density, and $\mu = \frac{1}{V} - 1$, where V is the relative volume, and e is the internal energy per unit volume. The parameters describing the water droplet in the analysis are tabulated in Table 1. The maximum and minimum smoothing length are considered as 2 and 0.2 respectively in the section definition card for SPH (defined as HMIN = 0.2 and HMAX = 2 in the *SECTION_SPH flag). A control flag is also added in the model for SPH elements, which includes the parameter such as MEMORY, which determines the number of neighbors initially defined for a particle, as well as FORM which includes the definition of a particle approximation theory to be used for the calculations.

The aluminum plate is modelled with single integration point constant stress solid element (ELFORM = 1) in LS-DYNA. Variable mesh sizing based on a mesh convergence analysis is used where the region near the impact is modelled finer with element size 0.04 mm x 0.04 mm. On the other hand, region away from the contact region is modelled coarser with element size 0.4 mm x 0.4 mm. Three elements through the thickness are used to discretised the aluminum plate. Given that the type of solid element uses a single integration point in the calculation, which is efficient from computational cost perspective, however, an hourglass control is added to the model to avoid any zero energy deformation modes. The aluminum plate is defined with *MAT_PIECEWISE_LINEAR_PLASTICITY material model, which is based on an elastic-plastic formulation and can be defined with an arbitrary stress versus strain curve. In the model, post elastic behaviour of aluminum is assumed linear and defined with a tangent modulus. The input parameters used in the model for aluminum are tabulated in Table 2. The bottom of the plate is constrained in all degrees of freedom, and the particles of the water droplet is defined with predefined initial impact velocity. As mentioned before, a node to surface penalty based contact algorithm is defined between the water droplet and aluminum plate. A time step scaling factor of 0.4 is added in the model (TSSFAC = 0.4 in the *CONTROL_TIMESTEP flag) which has been found suitable in literature [12] for fluid structure interaction using SPH formulations in LS-DYNA. This factor scales the time step during the simulation and improves the contact stability with soft materials [12,38] while providing sufficient accuracy.

4.2. Rain droplet impact modelling on the coating system

After the validation study, rain droplet impact modelling on the leading edge coating system is performed. A parametric study is considered to analyse the effect of (1) droplet diameters (2) impact angles and varying (3) impact velocities on the impact responses of the leading edge coating systems under different rainfall conditions. Following are the description of input parameters considered for the parametric analysis:

4.2.1. Rain droplet size

The size of droplet used for the analysis is an important parameter as different droplet size imparts different magnitude of damage to the material [40]. The droplet size for the analysis is chosen based on different rainfall conditions a wind turbine blade is expected to face during its operation phase. The rain drop size distribution used in this study is based on the model developed by [41] where the cumulative distribution function (CDF) of droplet diameters is related with the rainfall intensity by:

$$F(\phi_d) = 1 - e^{-\left(\frac{\phi_d}{1.3*I^{0.232}}\right)^{2.25}} \tag{8}$$

where ϕ_d is the droplet diameter in mm, and $I$is the rainfall intensity expressed in mm/hr. In this study, four different rainfall intensities are considered for the analysis and the corresponding probability density function (PDF) for the rain droplet size are presented in Fig. 8(a). These four rainfall intensities represent different classes of rainfall, i.e., 2 mm/hr represents light rainfall, 10 mm/hr represents moderate rainfall, 25 mm/hr represents heavy rainfall where as 50 mm/hr represents very heavy rainfall. A representative droplet diameter, which corresponds to the expected value of the rain droplet size (CDF = 0.5) for a given rainfall condition is chosen for the analysis (Fig. 8(b)). Therefore, rain droplet size (ϕ_d = 2.74 mm, 2.34 mm, 1.90 mm, 1.30 mm) are considered for impact with leading edge coating system and details are mentioned in Table 3.

4.2.2. Impact velocity and droplet impact angle

The impact velocity ($\vec{V}_{imp}$) considered in this study is defined as the relative velocity between blade tip velocity ($\vec{V}_{blade}$) and terminal velocity for the rain droplet which is given by:

$$\vec{V}_{imp} = \vec{V}_{blade} - (-\vec{V}_{tg}) \tag{9}$$

Table 1
Properties for water droplet and EOS_Gruneisen parameters [39].

ρ	v_s	C	a	S1	S2	S3
1000 kg/m^3	0.001 Pa.s	1480 m/s	0	2.56	−1.986	0.226

Table 2
Properties for Aluminum [39].

ρ	E	$\bar{\nu}$	σ_y	G
2820 kg/m^3	70000 MPa	0.3	240 MPa	27000 MPa

where the magnitude of $\vec{V}_{blade}$ is considered in the range of 80 m/s to 140 m/s at a step size of 20 m/s, whereas $\vec{V}_{tg}$ is the terminal velocity of the rain droplet i.e, the velocity with which the rain droplet falls onto the wind turbine blade. An empirical relationship between the terminal velocity and rain droplet size is given by [28]:

$$\vec{V}_{tg} = 9.65 - 10.3e^{-0.6\phi_d} \quad (0.5\text{mm} < \phi_d < 5\text{mm}) \tag{10}$$

where ϕ_d is the droplet size in mm and $\vec{V}_{tg}$ is the terminal velocity of the rain droplet in m/s. Fig. 8(c) presents the terminal velocity variation with the rain droplet size and the point where the black dotted line intersect the curve represents terminal velocity for a droplet in a given rainfall condition. Additionally, given that rain droplets impact the leading edge at different impact angles during operation, four different angles of impact between the rain droplet and leading edge coating systems are considered (30°, 45°, 60°, 90°). The details of the cases considered in this study for parametric investigation are summarised in Table 3.

4.2.3. Gelcoat and corresponding material model

An epoxy-based thermosetting polymeric resin Epon E862 is used as the gelcoat material in this work. The properties of coating material have been thoroughly investigated by [42] where a series of experiments were performed to characterise their tensile, compressive and shear properties at various strain rates and at different temperatures. The tests were carried out as per the ASTMD638 standards [43], and optical methods were used to include different strain rates [12]. Figs. 9(a)-(b) present the tensile and compressive engineering stress-strain curves for Epon E862 and it can be seen that the material's compressive strength is larger than it's tensile strength, and the material response is highly sensitive to the effect of strain rate. Also, at higher strain rates, material exhibits higher compressive and tensile strength. Consequently, a material model *MAT_PLASTICITY_COMPRESSION_TENSION from LS-DYNA material library is used for modelling the material response of the gelcoat material. This material model has been used by [12] for impact modelling on gelcoat material and the model allows tensile and compressive stress-strain data to be included individually together with the effects of strain rate. Strain rate can be included in the model either by using (1) Cowper-Symonds parameters, or (2) by using Eyring's equation where scaling effect on the yield stress with respect to strain rate is defined.

Generally, for plastics, it has been shown in the literature [44] that Eyring model predicts the strain rate behaviour of plastics better than Cowper-Symonds model (being inefficient in scaling the plasticity curve for plastics), and therefore the Eyring's model is considered in our study. The Eyring's model basically characterizes a linear increasing relationship between yield stress and strain rate, and is added through a tabular data using the LCSR flag (for both compressive (LCSRC) and tensile properties (LCSRT)). Here, the strain rate dependency of the yield stress, is implemented by defining the scaling factors for yield stress with strain rate. For obtaining these scaling factors, a linear curve is fitted to relate the yield stress for a given (measured) strain rate (Fig. 9(c)) defined by the equation:

$$\sigma_y = c\ log(\dot{\epsilon}) + k \tag{11}$$

where, σ_y is the yield stress for a measured strain rate $\dot{\epsilon}$, c and k are the slope and intercept of the line. One of the main advantage of using

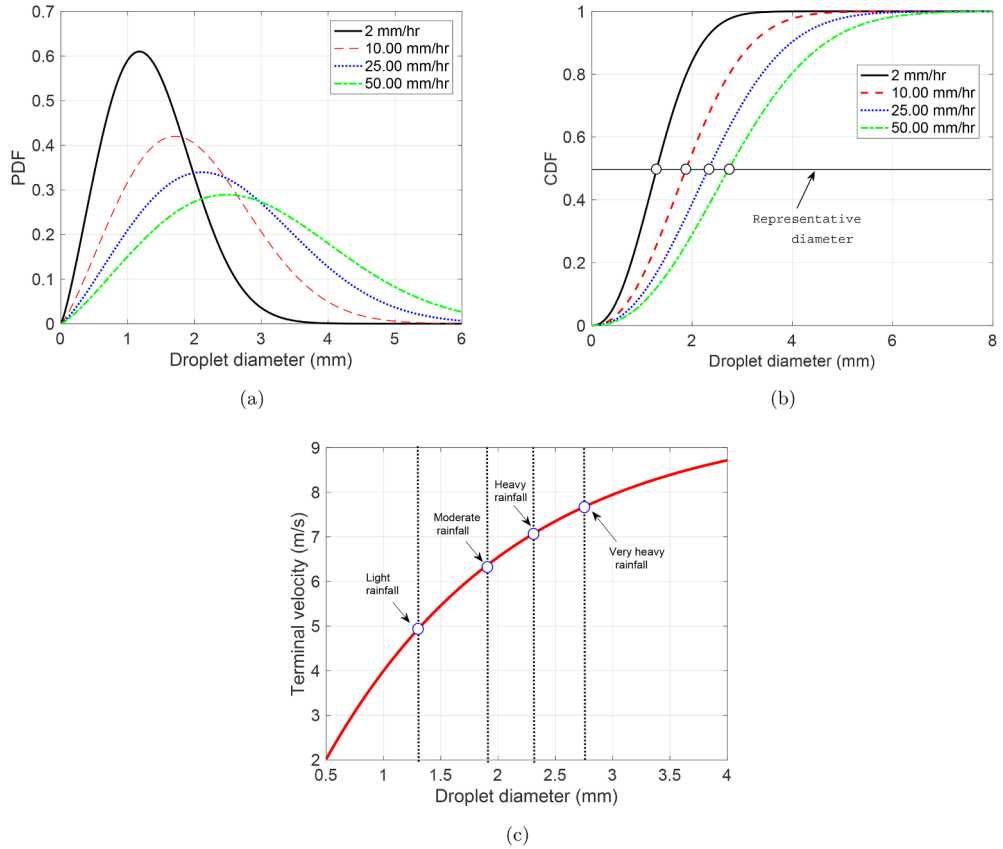

Fig. 8. (a) PDF of droplet size corresponding to four rainfall intensities (b) Cumulative distribution function (CDF) of droplet size and their expected value (c) Terminal velocity variation with droplet size.

Table 3
Parameters considered for analysis.

Rainfall condition	ϕ_d (mm)	$\vec{V}_{tg}$ (m/s)	$\vec{V}_{blade}$ (m/s)	$\vec{V}_{imp}$ (m/s)	α (degree)
1. Light Rainfall	1.30	4.93	80, 100, 120, 140	84.93, 104.93, 124.93, 144.93	30°, 45°, 60°, 90°
2. Moderate Rainfall	1.90	6.35	80, 100, 120, 140	86.35, 106.35, 126.35, 146.35	30°, 45°, 60°, 90°
3. Heavy Rainfall	2.34	7.12	80, 100, 120, 140	87.12, 107.12, 127.12, 147.12	30°, 45°, 60°, 90°
4. Very heavy Rainfall	2.74	7.66	80, 100, 120, 140	87.66, 107.66, 127.66, 147.66	30°, 45°, 60°, 90°

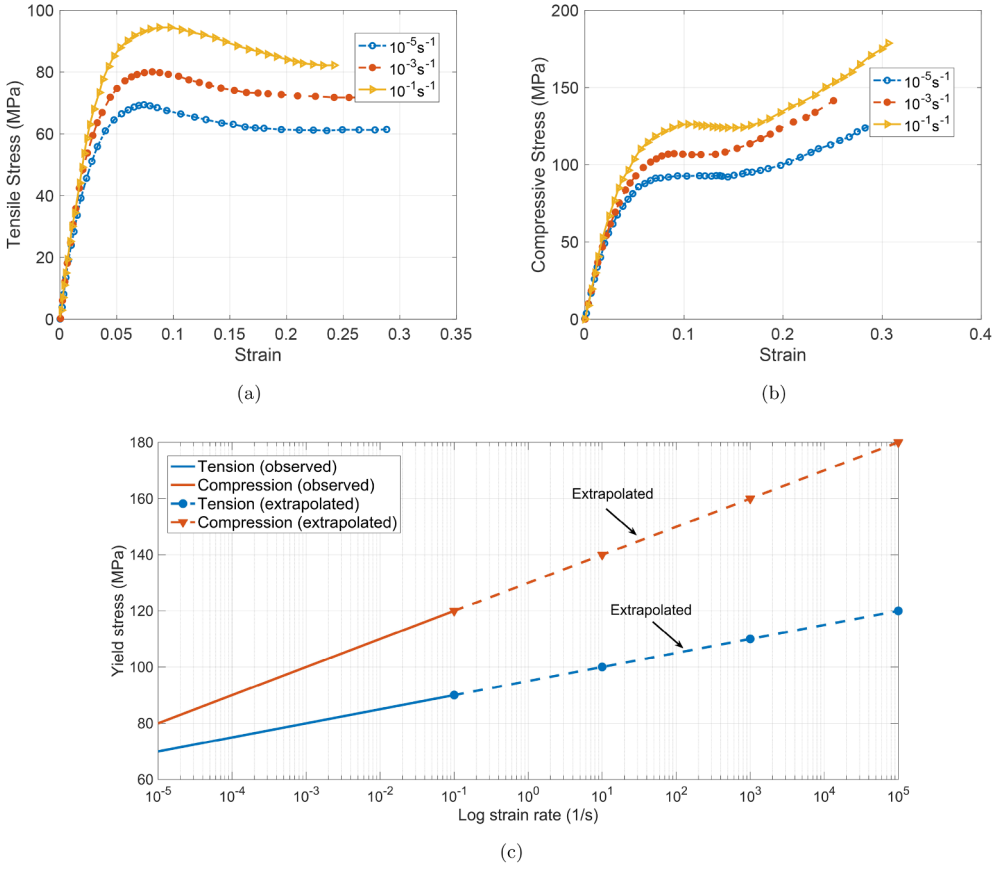

Fig. 9. Epon E862 material properties: (a) Tensile stress-strain curve [42] (b) Compressive stress–strain curve [42] (c) Variation and extrapolation of yield stress of the material at different strain rates.

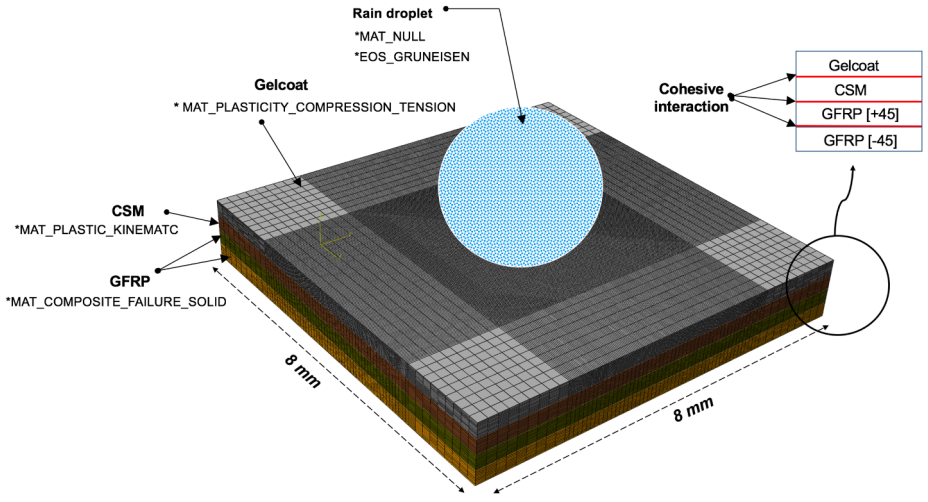

Fig. 10. Numerical model for rain droplet impact on leading edge coating system.

Eyring equation is that the strain rate scaling effect can be extrapolated for higher values, in case the data is not available for higher strain rates (as shown in Fig. 9(c)). A similar approach is considered in [44], where impact simulations on acrylic and polycarbonate polymers were performed. The coating thickness for the gelcoat layer is taken as 0.3 mm ($t_c = 0.3$mm) and is based on recommendation made by design guidelines [33].

4.2.4. Numerical model for rain droplet impact and the parametric study

A numerical model capable of simulating a single rain droplet impact on the leading edge coating system is developed in LS-DYNA code. SPH modelling was automated using a script where it was possible to vary the droplet sizes, impact angles as well as impact velocities for parametric impact investigation. Fig. 10 presents the numerical model developed for the rain droplet impact on the leading edge coating system for one of the cases. A leading edge coating system of dimension 8 mm × 8 mm is considered having - (a) a gelcoat layer on the top, (b) followed by CSM (chopping strand mat), and (c) one layer of biaxial Glass Fiber Reinforced Plastic (E-GFRP) consisting of [+45/−45] plies. The rain droplet is discretised with SPH particles, and is defined with *MAT_NULL material model, together with Gruneisen based EOS model (Table 1). On the other hand, the leading edge coating system is modelled with one point constant stress solid element. Gelcoat material is modelled with *MAT_PLASTICITY_COMPRESSION_TENSION and strain rate effects are included. The material properties used in the analysis for the gelcoat layer include tensile and compressive stress-strain curves together with values mentioned in Table 4. The chopping strand mat (CSM) is added below the gelcoat layer and consists of randomly oriented fibers which are distributed uniformly on top of the blade laminate. Therefore, CSM layer can be assumed to exhibit isotropic properties, and *MAT_PLASTIC_KINEMATIC material model is used. This material model is effective for modelling material with isotropic and kinematic hardening plasticity behaviour and the properties used in the analysis for CSM are mentioned in Table 5. Finally, the composite biaxial layers are modelled individually into two separate layers with [+45/−45] orientations and are defined with *MAT_COMPOSITE_FAILURE_SOLID material model. The material model can consider progressive damage in the composite based on a three dimensional stress based failure criterion and can predict (1) longitudinal, transverse and through-the-thickness compressive failure, (2) longitudinal and transverse through-the-thickness shear failure, and (3) tensile failure in the longitudinal direction [12,38]. The composite substrate used in this study is based on an E-GFRP composite made of HiPer-Tex E-Glass fiber and momentive epikote resin and the details of the material property implemented in the analysis is given in Table 6. The contact interaction between the rain droplet and the top gelcoat layer is defined using particle to surface contact algorithm where the fluid particle is defined as the slave, and the coating layer is defined as the master. In addition, contact formulation in the form of cohesive interactions are defined between different layers of the coating system through use of *CONTACT_AUTOMATIC_SURFACE_TO_SURFACE_TIEBREAK together with OPTION = 6 to model any potential interfacial delamination. The advantage of OPTION = 6 in LS-DYNA is that this formulation does not require detailed fracture toughness data and interlaminar behaviour is defined in terms of normal and shear strength parameters. Nodes between the individual layers are initially tied with each other preventing any sliding motions, and once the failure criterion is met, delamination initiates. The failure criterion for the formulation is given by:

$$\left(\frac{|\sigma_n|}{NFLS}\right)^2 + \left(\frac{|\sigma_s|}{SFLS}\right)^2 \geqslant 1 \tag{12}$$

where, σ_n and σ_s are the normal and shear stresses acting on the interfaces respectively. *NFLS* and *SFLS* are interlaminar normal and shear strength respectively.

4.2.5. Analytical-numerical verification of rain droplet impact on leading edge coating system

Although a validation study is carried out to compare the results of the developed coupled fluid structure interaction (FSI) computational model (as discussed in Section 4.1), an analytical-numerical verification is performed to validate the model used for rain droplet impact on leading edge coating system. The verification study is based on the work of Zhang et al. [46,47], where extensive experiments were carried out for droplet impact on solid surface. Analytical expressions were derived for peak impact forces (F) and impulses (I) generated on the solid surface for the case of impact with droplets of different sizes, several impact velocities and for different impact angles. These are given by:

$$F = 0.84\,\rho_w\,V_{imp}^2\,\phi_d^2 \tag{13}$$

$$I = 0.56\,V_{imp}^{0.95}\,\phi_d^{2.98} \tag{14}$$

Note that the equations presented above are valid as long as the droplet is assumed spherical, and the droplet impact lies in the inertial dominated regime characterized by a Reynolds number (R_e) greater than 230 and Weber number (W_e) greater than 50. These limits were valid for all the cases considered in our study and thus these equations can be used. For the present study these parameters are:

$$R_e = \frac{\rho_w V_{imp}\phi_d}{\mu} > 230; \quad W_e = \frac{\rho_w V_{imp}^2\phi_d}{\gamma} > 50 \tag{15}$$

where ρ_w, μ, γ are density, viscosity coefficient and surface tension respectively, which is for water taken as 1000 kg/m^3, 0.001 Pa.s and 73.42 mN m^{-1} in this study. Moreover, since the impact lies in the inertia-dominated region, the effects of viscosity and surface tension are less significant and can be neglected in the numerical model.

4.2.6. Numerical model for repetitive rain droplet impact

The main goal of the repeated rain droplet impact analysis is to compare the number of impacts required for initiation of erosion damages for different blade tip velocities and to quantify the efficiency of controlling LEE in case the rotor speed is reduced. This information is vital for developing control algorithm for reducing tip speed of the blade during harsh precipitation. To achieve this, we utilised a method already used in the literature [12] for rain droplet impact on the gelcoat-based coating system. The novelty of the method, however, is an automated script that did the work of repetitive impact compared to the literature [12] where multiple raindrops were stacked on top of each other for analysis (which is computationally demanding for an explicit solver). A restart script is developed for performing repetitive rain droplet impact in LS-DYNA code. The stress and strain state together with damage status of the coating material due to current droplet impact is transferred to the next analysis for subsequent rain droplet impact. A binary dump file is written at the end of the analysis which consists of stress and strain history of the leading edge coating system. A full restart input deck consisting of the original master model is used and the stress and strain history is added as an initial condition on the coating model for the subsequent impact. Preexisting contact formulations such as cohesive interactions between the layers of leading edge coating systems as well as node to surface interaction between droplet and gelcoat layer are retained in the analysis. In this way, erosion state of the leading edge system due to repeated rain droplet impact is simulated. Erosion on the leading edge coating material is defined at the point where the effective plastic strain in the gelcoat layer matches with

Table 4
Properties for Gelcoat layer [12]

ρ	E	$\bar{\nu}$	σ_y^t	σ_y^c
1150 kg/m^3	2500 MPa	0.4	90 MPa	120 MPa

Table 5
Properties for CSM [12]

ρ	E	$\bar{\nu}$	σ_y
1452.8 kg/m^3	8 GPa	0.3	190 MPa

the failure strain (0.3). A *MAT_ADD_EROSION card is added in the material library and the element is deleted if the erosion criteria is fulfilled. In this study, the effect of ten repetitive rain droplet impact is considered and number of impacts for onset of erosion damages in the gelcoat layer are predicted and compared for different blade tip velocities.

5. Results and discussion

In this section, the results for the validation study are presented first, where response parameters from numerical simulations are compared against experimental observations from [39]. These are followed by the parametric study results dealing with single rain droplet impact on leading edge coating system. An analytical numerical verification of these results are also presented. Finally, erosive state of the coating material subjected to repetitive rain droplet impact are examined, and number of impact for onset of erosion are compared for different blade tip velocities.

5.1. Validation study

To obtain results which are independent of mesh size effects, a mesh convergence study is performed for the number of particles required to discretise the water droplet. Fig. 11 presents the comparison of impact forces obtained in the numerical study by varying the number of SPH particles from 50 k to 150 k. The results show that the difference between the measured value from the experiment [39] and numerical simulation reduces with increasing number of SPH particles, with acceptable differences obtained with 130 k particles. Any further increase in the number of particles is found to have negligible effect on the difference between the observed and the calculated values, and therefore 130 k number of SPH particles is considered for the analysis. Impact investigations are then performed for different droplet diameters and impact velocities and critical response parameters such as - (a) droplet morphology (b) contact forces and (c) impulses - are analysed and presented below.

Fig. 12 presents the qualitative comparison of droplet morphology i.e., the droplet shape during different stages of impact, between experiments (from [39]) and numerical simulations for the case where the droplet diameter of 2.7 mm impacts the aluminum plate with 2.67 m/s. The contact between the droplet and aluminum plate initiates at 0 μs, with no record of water jetting or spreading till 50 μs in both experiment and numerical simulations. However, the phenomenon of water jetting or spreading becomes more pronounced after 100 μs and can be clearly seen at 200 μs. It is evident in both the comparison that the contact area between droplet and plate gradually increases whereas the droplet height decreases with time. Overall, the numerical model presents a good agreement with the experiments in terms of droplet morphology and replicates the droplet behaviour during its impact on the aluminum plate.

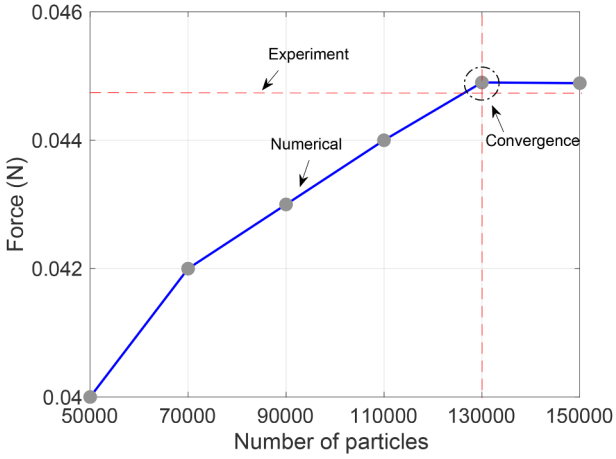

Fig. 11. Particle convergence study.

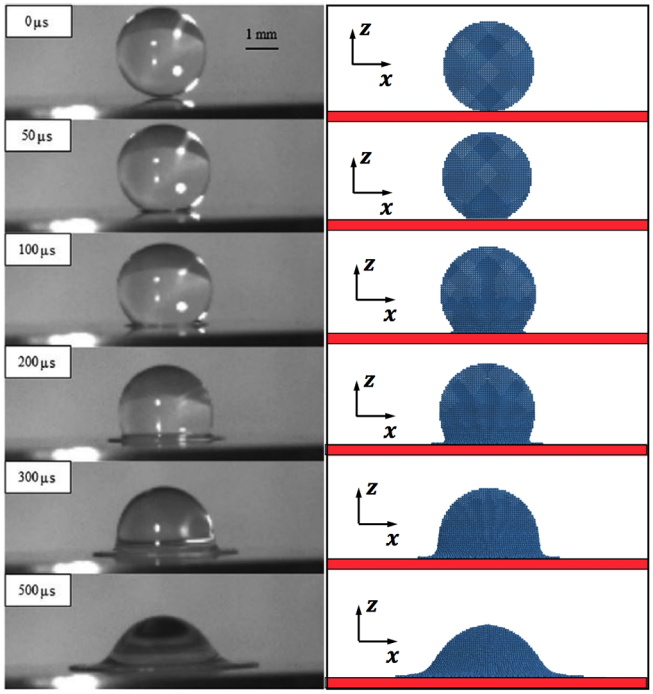

Fig. 12. Comparison of droplet morphology between experiments [39] and numerical simulation (same scale is used for comparison).

Fig. 13(a) further presents the quantitative comparison between the contact forces obtained from the numerical simulation with the observed value from the experiment for the case where the droplet diameter of 2.7 mm impacts the aluminum plate with 2.67 m/s. First of all, both the curves present a reasonable fit with each other, with both curves showing a sharp rise in the contact forces at the instant of contact initiation, and a relaxed declining stage post the maximum

Table 6
Properties for unidirectional E-GFRP composite [45]

ρ	E_{11}	$E_{22} = E_{33}$	$\bar{\nu}_{12} = \bar{\nu}_{13}$	$\bar{\nu}_{23}$	$G_{12} = G_{13} = G_{23}$	X_T
1864 kg/m^3	44.87 GPa	12.13 GPa	0.3	0.5	3.38 GPa	1006.3 MPa
X_C	$Y_T = Z_T$	$Y_C = Z_C$	$S_{12} = S_{13} = S_{23}$	NFLS	SFLS	
487 MPa	45.95 MPa	131.90 MPa	49.51 MPa	45.95 MPa	49.51 MPa	

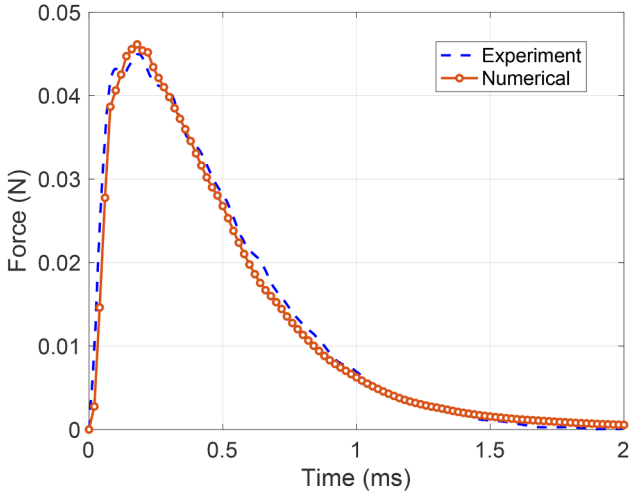

(a)

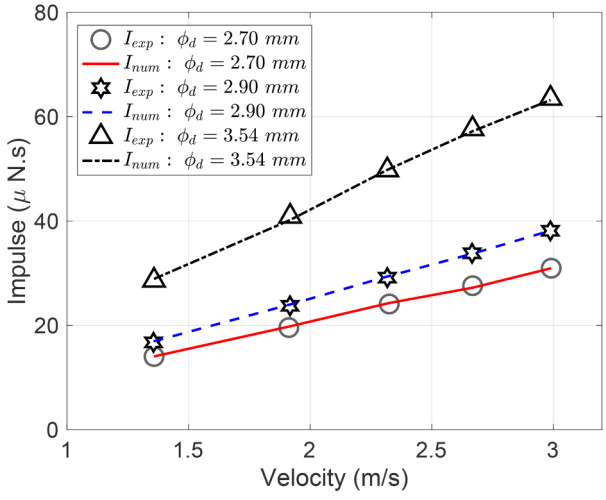

(b)

Fig. 13. (a) Comparison of contact forces for ϕ_d = 2.7 mm and V_d = 2.67 m/s (b) Comparison of impulses for various cases of droplet size and impact velocity.

value. Further, the maximum contact forces measured from the experiments and estimated from numerical simulations are in good agreement, with a difference of 2.1% in the numerical simulation. Finally, different cases of droplet diameters are considered together with varying impact velocities, and a comparison of impulses between experiment and numerical simulation is shown in Fig. 13(b). For obtaining impulses, contact-force time history curves are numerically integrated to obtain the underlying area (duration over which the contact force acts) and it can be seen that the impulse of the water droplet on the aluminum plate increases with increasing impact velocity and increasing droplet size. Also, a good fit is seen between the experiment [39] and calculated values from the simulation for all the cases, thereby confirming a sound validation of parameters used in the numerical model.

5.2. Rain droplet results on the leading edge coating system

In this section, discussion on rain droplet impact investigation on the leading edge coating system will be presented. As detailed in Section 3.4, different parameters are considered in the analysis such as (1) droplet diameters (ϕ_d = 2.74 mm, 2.34 mm, 1.90 mm, 1.30 mm) corresponding to different rainfall intensities (b) droplet impact angles (α = 30°, 45°, 60°, 90°), and (c) varying impact velocities (V_{blade} = 80, 100, 120, 140 m/s). Repetitive rain droplet impacts are considered and the erosive states on the leading edge coating system are compared for different blade tip velocities. First, the impact responses and detailed rain droplet mechanism on the leading edge coating system is presented for a few critical cases, and finally the results for the parametric study are discussed.

5.2.1. Single impact of a rain droplet (Droplet diameter (ϕ_d) = 2.74 mm, Impact velocity (V_{imp}) = 107.6 m/s, Impact angle (α = 90°))

Here, the discussion is made with respect to rainfall intensity of 50 mm/h which corresponds to very heavy rainfall conditions and has a representative rain drop diameter of 2.74 mm. Fig. 14 presents the contact force history for a case where a single rain droplet impacts the leading edge coating system with V_{imp} = 107.6 m/s, and at normal impingement angle (α = 90°). It can be observed from the figure that there is a rapid increase in the contact forces at the time instant of contact initiation between droplet and the leading edge coating system, followed by an oscillatory behaviour of the curve, and finally a smooth decline of the force history. The contact-force curve explains critical stages of rain droplet impact and is marked with different label pointers from A-H (Fig. 14), the details of which are discussed below.

At the beginning of the contact initiation where the droplet impacts the leading edge coating system, there is development of water hammer pressure (time duration of less than 1 μs) and is represented by the stages A-B in the contact-force curve. The droplet behaviour during the water hammer stages (A-B) is presented in Fig. 15 in terms of its velocity contour plots. It can be seen that the rain droplet upon contact initiation decelerates rapidly and there is an instant volumetric compression of the rain droplet. This stage is also called as initial compressible stage and induces water hammer pressure together with

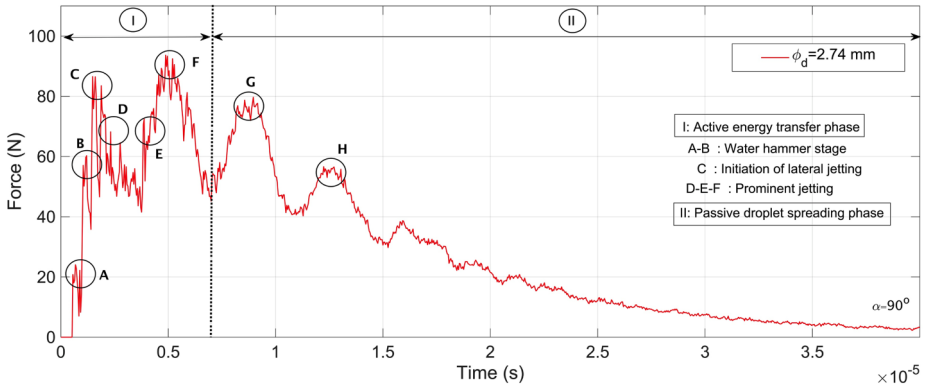

Fig. 14. Contact force history for rain droplet impact on leading edge coating system for the case- ϕ_d = 2.74 mm, V_{imp} = 107.6 m/s, α = 90° (Stage *I*: active energy transfer phase, Stage *II*: Rain droplet spreading phase).

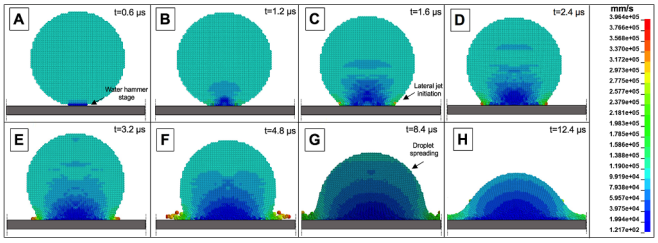

Fig. 15. Velocity contour plot of rain droplet at different stages of contact force history.

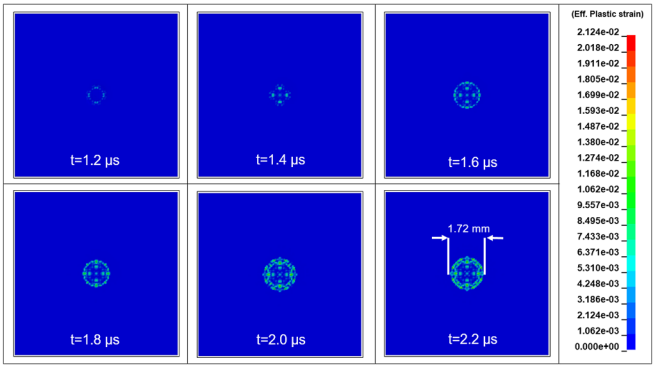

Fig. 17. Effective plastic strain contour plot at leading edge coating system at various stages of contact force history (ϕ_d = 2.74 mm, V_{imp} = 107.6 m/s, α = 90°).

subsequent first peak in the contact-force curve at stage B. Fig. 16 presents the Rayleigh (surface) stresses on the coating surface during the water hammer stages (A-B). The contour plot shows the initiation of surface stresses on the coating layer at the stage of contact initiation, with local high stresses (close to 120–125 MPa) developed in circular pattern at the contact area of the coating system at stage B. It is to be noted that maximum surface stress during water hammer stage is found just above the yield stress for the gelcoat layer, presented in Table 4, thereby contributing to the initiation of plastic strain. This can also be observed in Fig. 17 where effective plastic strain can be observed at approximately 1.2 μs of the contact duration, which matches with the water hammer stage.

After the water hammer stage of the droplet impact which lasts for less than 1 μs, a stage of lateral jetting initiation in the droplet begins at stage C, which becomes prominent at stages D, E and F. During this stage, high pressure developed in the droplet during the water hammer stage is released, thereby inducing high velocity flow of the liquid in the radial direction. This is shown in Fig. 15, where at frames C, D, E and F of the jetting stage, the velocity of the rain droplet at its lateral edges is found to have increased by almost two to four times relative to the initial impact velocity. The lateral jetting stage also changes the nature of surface stresses induced onto the coating with concentrated peak stresses developed in a concentric ring pattern. These stresse induces local deformation of the gelcoat layer, which further interacts with rayleigh surface stresses to develop peak stress of around 150 MPa and subsequent increased plastic strain on the coating layer. Note that surface stresses developed in the coating are considerably beyond the yield stress for the gelcoat material, presented in Table 4, rendering further development of plastic strain. Therefore, it is found that the lateral jetting stage of the rain droplet impact contributes maximum to the damage of the gelcoat layer. It is to be also noted that water hammer stage of the droplet impact is crucial and plays a significant role during droplet impact by: (a) causing a rapid increase in the stresses of the coating surface during initial stages which may cause minor yielding of the gelcoat layer, and by (b) generating rayleigh waves onto the coating surface which in later stages interacts with droplet jetting phase to develop subsequent damage progression. This finding agrees reasonably well with the observations made in the literature [12].

Finally, the droplet transfers all of its significant kinetic energy onto the leading edge coating system and a secondary spreading stage of the rain droplet is seen at stages G and H of the contact force curve. The stress contour plot for the coating layer (Fig. 16) shows that almost all the surface stresses developed due to droplet impact are attenuated at stages G and H.

In summary, the contact-force curve during the rain droplet impact on the leading edge coating system can be distinguished into two distinct stages for describing the erosion behaviour (Fig. 14) – the first stage (1) represents the active energy transfer phase where the maximum load share from the rain droplet impact is transmitted onto the leading edge coating system (A-F). This stage is responsible for phenomena such as – development of water hammer pressure due to compressed liquid upon contact (A-B), and onset and progression of droplet's lateral jetting due to subsequent pressure release (C-F). This

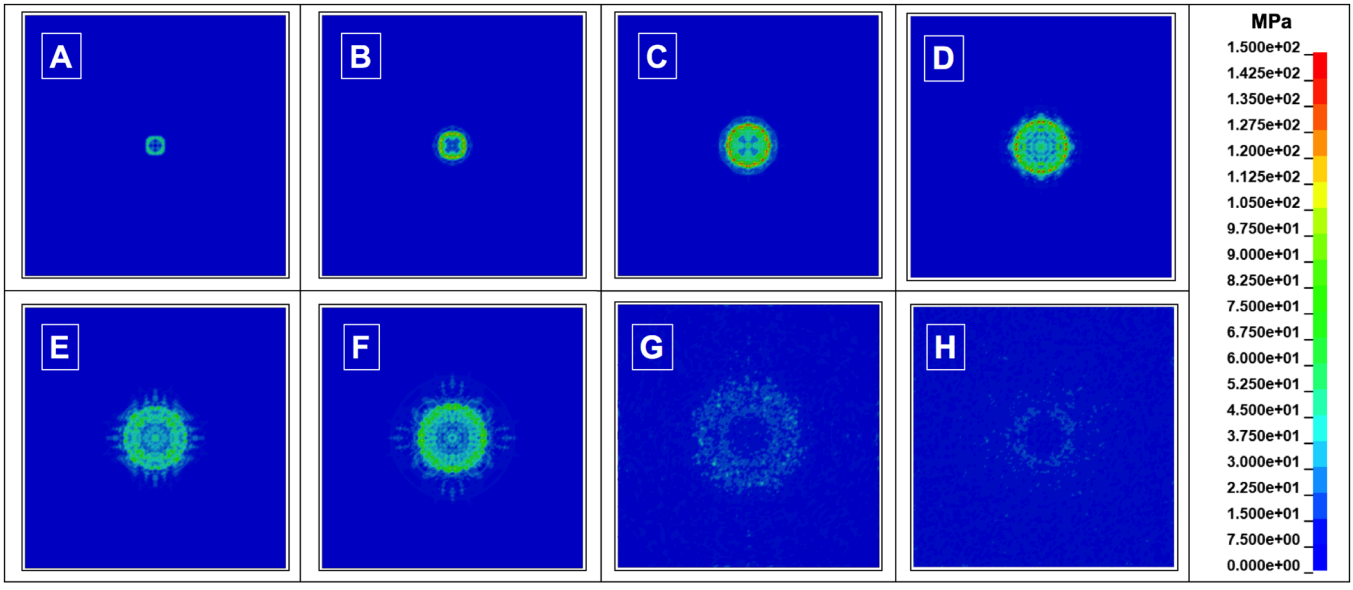

Fig. 16. Rayleigh surface stress contour plot at leading edge coating system at various stages of contact force history (ϕ_d = 2.74 mm, V_{imp} = 107.6 m/s, α = 90°).

stage is critical for the erosion of coating material and develops maximum damage due to rain droplet impact. On the other hand, the second stage (II) consists of rain droplet passive spreading phase (G-H-end), and there is no significant transfer of loads from rain droplet onto the coating system, thereby contributing negligibly to the erosion damages.

In order to verify how much the stiffness properties of the substrate affect the fluid-dynamics of the rain droplet impact, a comparative study was performed. The impact analysis was considered on just the gelcoat material and compared with the results presented before for the multilayered coating system. It was found that addition of substrate does not affect the result of impact responses. In addition, due to rain droplet impact on the coating system, majority of stresses are developed on the coating surface (Layer 1), while the substrates (consisting of CSM and composite layers) remain intact throughout the simulation. Therefore, the presence of substrates in the model is to merely provide a realistic representation of leading-edge coating system and boundary conditions. Further, no delamination is found to develop between the individual interfaces. It is to be also noted that this result is applicable for low energy impact related to rain droplet impact, and caution must be exercised for hail impact. During hail impact, the effect of substrate conditions must be analysed on the structural responses given that such collision involves high energy impact.

A contour plot of effective plastic strain developed on the coating surface due to rain droplet impact is presented in Fig. 17. The damage pattern in the coating exhibits a ring pattern which is representative of the observation made in the literature [12,26]. Also, maximum damage occurs during initial stages of droplet lateral jetting (within 2.2 μs) and lies in the active energy transfer phase (Stage I). Further, the maximum effective plastic strain developed in the coating due to rain droplet impact is 0.021, which is much less than the failure strain of 0.3 for the gelcoat material. This implies that single rain drop impact is not expected to cause erosion of the coatings. It is to be also noted that layers below the coating including the interfaces and composite layers remain intact and the effective plastic strain are restricted to the top surface of the coating material. This is in line with observations made in the literature where the dominating failure mode for gelcoat-type coating material is the erosion of its top surface [12].

5.2.2. Parametric study: Effects of droplet diameter, droplet impact angle, and impact velocity

Fig. 18(a) compares the impact force history for cases where a rain droplet having diameter (ϕ_d) = 2.74 mm impacts the leading edge coating system at different impact angles (α = 30°, 45°, 60°, 90°) and with an impact velocity (V_{imp}) = 107.6 m/s. The peaks in the contact-force history are largest for rain droplet impact with normal impingements (α = 90°) and further reduces with shift in the impact angle away from the normal impingement. For instance., the maximum contact forces for the case with normal impingement is around 93.7 N, which drops to 22.9 N for rain droplet impact with an angle of α = 30°. Further, the total contact duration which include active and spreading phase of the rain droplet during its impact on the coating system does not change with varying droplet impact angle.

Fig. 18(b) compares the impact force history for cases where the rain droplet with varying size (ϕ_d = 2.74 mm, 2.34 mm, 1.90 mm, 1.30 mm) impacts the leading edge coating system at normal

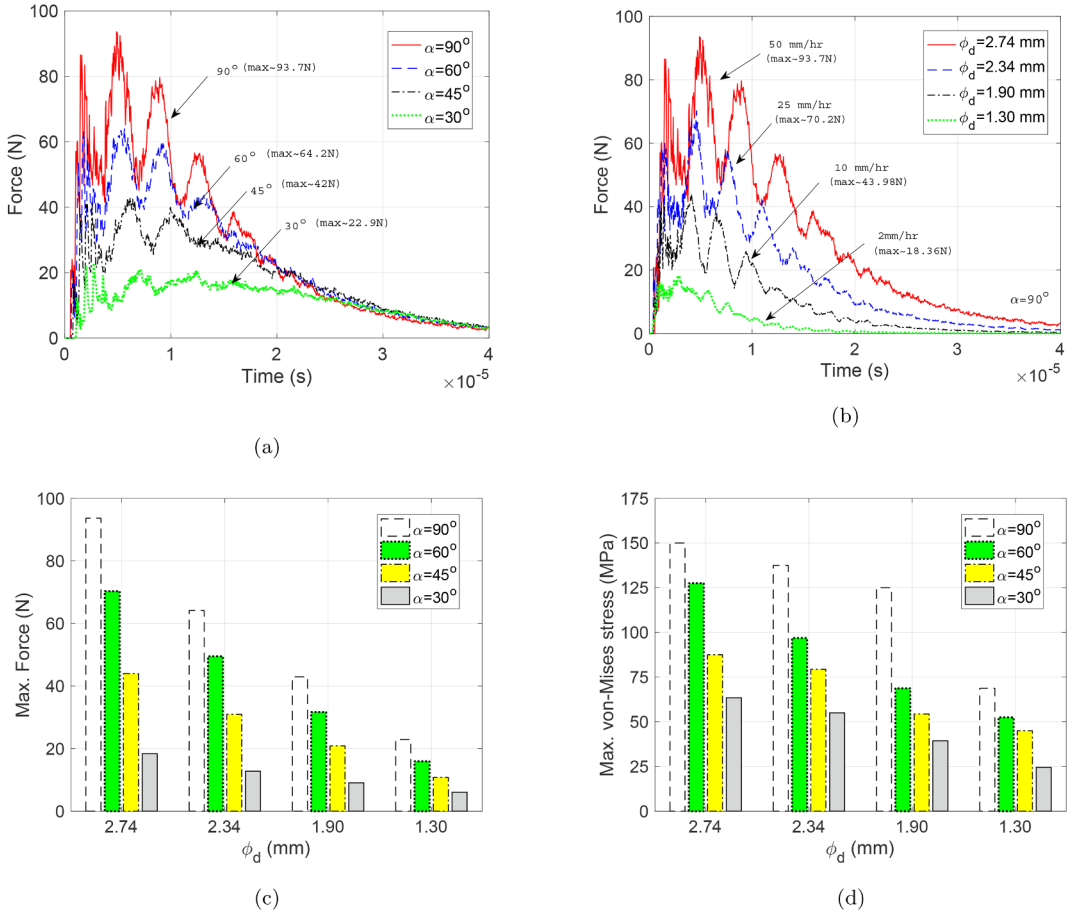

Fig. 18. Comparison of contact-force history for rain droplet impact: (a) ϕ_d = 2.74 mm, V_{imp} = 107.6 m/s and α = 30°, 45°, 60°, 90° (b) ϕ_d = 2.74 mm, 2.34 mm, 1.90 mm, 1.30 mm and α = 90°, V_{blade} = 100 m/s, comparison of (c) maximum contact forces (d) maximum von Mises stresses on the coating system.

impingement and with V_{blade} = 100 m/s. The peaks in the contact force history increases with increasing droplet diameter, for instance, maximum contact force for the case with ϕ_d = 1.30 mm is 18.36 N, which increases to 93.7 N for ϕ_d = 2.74 mm. Also, the contact durations are longer for larger droplet size and reduces with decreasing rain droplet diameter. This observation is in line with studies performed in the literature [48]. A comparison of the maximum contact forces and maximum von-Mises stresses for varying droplet diameters and droplet impact angles are presented in Fig. 18(c) and (d) respectively. The results clearly show that the impact responses of the leading edge coating system is dominated by the case of largest droplet size together with normal impingement. Fig. 19 presents the post impact contour plot of effective plastic strain developed in the coating layer for two different droplet impact angle (α = 90°, 60°) and for ϕ_d = 2.74 mm. It is found that for a given droplet size, the impact of the rain droplet on the coating system is more severe at normal impingements.

Figs. 20(a)-(d) compare the analytical impact force obtained using Eq. (13) with the maximum impact force obtained from numerical simulation, for the cases of different droplet diameters, different droplet impact angles considered along with blade velocity of 100 m/s. The results obtained from the numerical study are in satisfactory agreement with the analytical formulation for all the cases as seen in the figures, however, are slightly overstimated while using the numerical simulation. Nevertheless, the trend in the contact force history is in complete agreement with the analytical results for all the cases (lying closely to the black curve), thus indicating a sound verification of the numerical model.

Response surface method (RSM) is utilised to develop an analytical relationship between impulses developed on the leading edge coating system due to rain droplet impact and erosive variables like droplet diameter (ϕ_d) and impact angle (α). RSM is an ensemble of statistical techniques by which analytical relationship can be derived for an output response variable which is related with multiple independent response variables. Numerical integration of force-time history is performed for different cases of droplet size (ϕ_d) and droplet impact angle (α) to obtain impulses on the leading edge coating system. In total there were 16 data points for response surface estimation (4 × 4, combination of 4 values for ϕ_d and 4 values for α) and are fitted with linear, quadratic, cubic as well as quartic models. The accuracy of these fits are checked by comparing Root Mean Square Error (RMSE) and coefficient of determination (R^2). It is found that impulses are related to droplet diameter and impact angle through a cubic model and the obtained response surface impulse equation had in total 10 terms. Figs. 21(a)-(b) present the 3D and 2D response surfaces for the impulses developed on the leading edge coating system which shows that these values increases with increasing droplet size and are largest for normal impingement. Further, the 2D-response surface for the impulses also show that the effects of rain droplet impacting the leading edge coating system at inclined impact angles (50° to 90°) are critical for rainfall

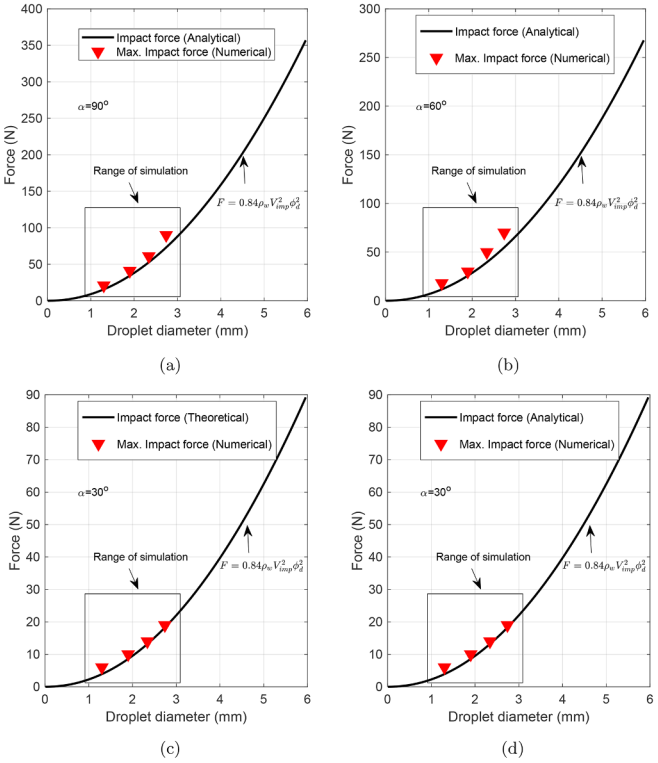

Fig. 20. Comparison of peak impact forces obtained from analytical [46] and numerical model for rain droplet impact on the gelcoat surface: (a) α = 90° (b) α = 60° (c) α = 45°(d) α = 30°, for ϕ_d = 2.74 mm, V_{blade} = 100 m/s.

intensity greater than 25 mm/hr (representing very heavy rainfall conditions). For instance, the impulse developed due to droplet size ϕ_d = 2.74 mm (very heavy rainfall condition) and α = 50° is larger than impulse developed on the coating due to impact with droplet size ϕ_d = 1.30 mm (light rainfall) and normal impingement (α = 90°). In summary, inclined impact angles are crucial erosive variables for rain erosion analysis, especially dealing with high intensity rainfall conditions. Also, the impulses obtained from the analytical formulation using Eq. (14) is presented in Fig. 21(c) and can be compared with the Response Surface (RS) of the impulse obtained from numerical simulation. A very good agreement is seen with the results obtained from the numerical simulation for all the cases (and for all rainfall conditions); with numerical analysis overestimating the impulses slightly by around 3–5%. Nevertheless, these results indicate a satisfactory verification of the numerical model developed in LS-DYNA.

Fig. 22(a) presents the comparison of contact forces for the case where droplet size (ϕ_d = 2.74 mm) corresponding to very heavy rainfall

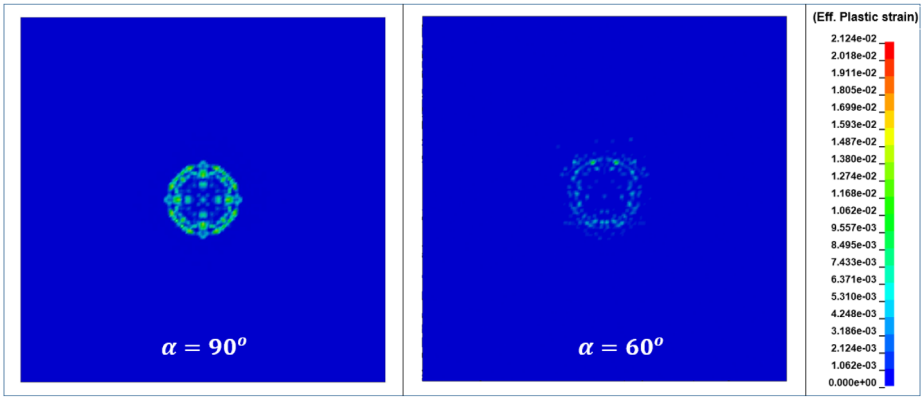

Fig. 19. Comparison of effective plastic strain at the gelcoat layer due to rain droplet impact for the case ϕ_d = 2.74 mm, V_{imp} = 107.6 m/s and α = 90°, 60°.

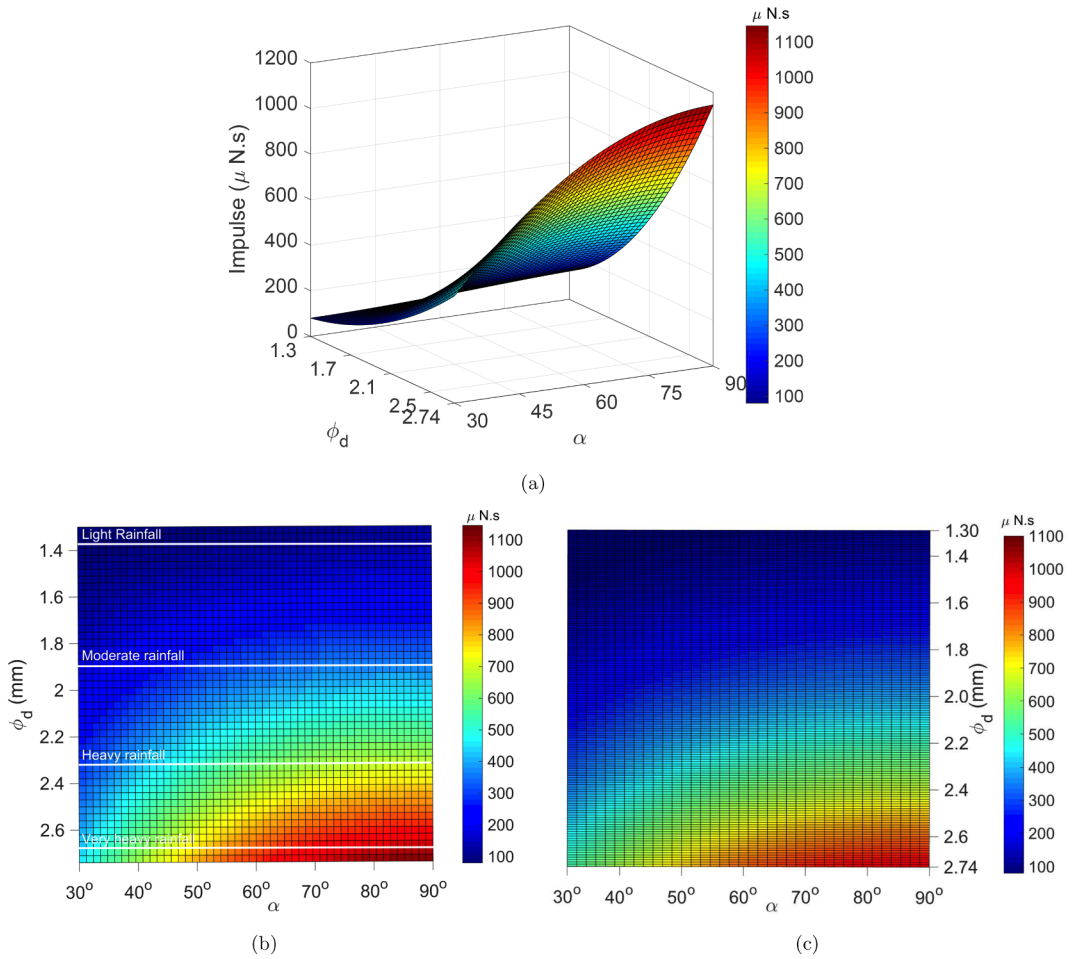

Fig. 21. (a) 3D and (b) 2D response surface for impulse (obtained from numerical simulation) on the leading edge coating system and related to rain droplet erosive variables: ϕ_d and α (c) Impulses obtained on the gelocat surface using analytical formulation from [47].

condition, impacts the leading edge coating system with different impact velocities (V_{blade} = 80, 100, 120, 140 m/s) and at normal impingement ($\alpha = 90°$). Contact forces are highest for largest impact velocities and reduces with decrease in the impact velocity. For instance, maximum impact force for the case of V_{blade} = 140 m/s is 181 N, which reduce to 69.35 N for V_{blade} = 80 m/s, thereby a reduction in the maximum impact force by more than 70%. This clearly indicates the merit of developing control algorithms for reducing blade tip speed during harsh precipitation as the impact forces are significantly reduced. Fig. 22(b) presents the 2D response surface for contact forces and relates erosive variables - blade tip speed (V_{blade}) and droplet size (ϕ_d) (corresponding to different rainfall intensities). Different response surface models are checked and cubic model gave the best fit. Impact forces on the leading edge coating system increase with increasing rainfall intensity as well as increasing blade tip velocities. Fig. 22(c) presents the comparison of maximum effective plastic strain developed in the gelcoat layer due to rain droplet impact having different droplet sizes and different impact velocities. The maximum effective plastic strain is highest for the largest droplet size and highest blade tip velocity. All in all, the impact responses on the coating system due to single rain droplet impact increase with increasing droplet size, droplet impact angle, rainfall intensity and blade tip velocity.

5.2.3. Repeated rain droplet impact and estimation of erosion onset

It has been discussed already that the maximum effective plastic strain developed in the gelcoat layer due to single rain droplet impact is much less than the material's failure strain for even the most critical cases of rainfall conditions. Therefore, the case of single rain droplet impact is not expected to develop erosion damages on the leading edge coating system. In order to simulate the erosive state of the leading edge coating system, as well as to predict the number of impacts required for the onset of erosion damage, a numerical model for repetitive rain droplet impact is utilised. Ten repetitive rain droplet impact are considered at the same location on the leading edge coating system, and the maximum effective plastic strain (ϵ) is related with the number of impacts (n) using regression analysis. After these variables are fitted with a suitable regression model, number of impacts to the onset of erosion damages is predicted by extrapolating the regression curve to a value corresponding to the failure strain of the gelcoat material. Also, the number of impacts to erosion damage is compared for varying blade tip velocities.

Fig. 23 presents the contour plot of effective plastic strain developed in the gelcoat layer due to four repetitive rain droplet impact for the case of ϕ_d = 2.34 mm, V_{blade} = 100 mm, and normal impingements $\alpha = 90°$. It is found that maximum effective plastic strain as well as the total extent of damage in the gelcoat layer increases with increasing number of rain droplet impacts. Also, maximum damages are obtained in concentric rings around the contact area and this is in line with the observation made in the literature [26] for the damage pattern on the gelcoat layer. Fig. 24(a) presents the cumulative maximum effective plastic strain developed in the leading edge coating system due to ten repetitive impacts. The maximum effective plastic strain corresponding to each number of impacts are filtered out and is related to number of impacts (n) with a linear regression model. It can be seen from Fig. 24(b) that the effective plastic strain (ϵ) is related to number of impacts (n) satisfactorily through a linear model with equation

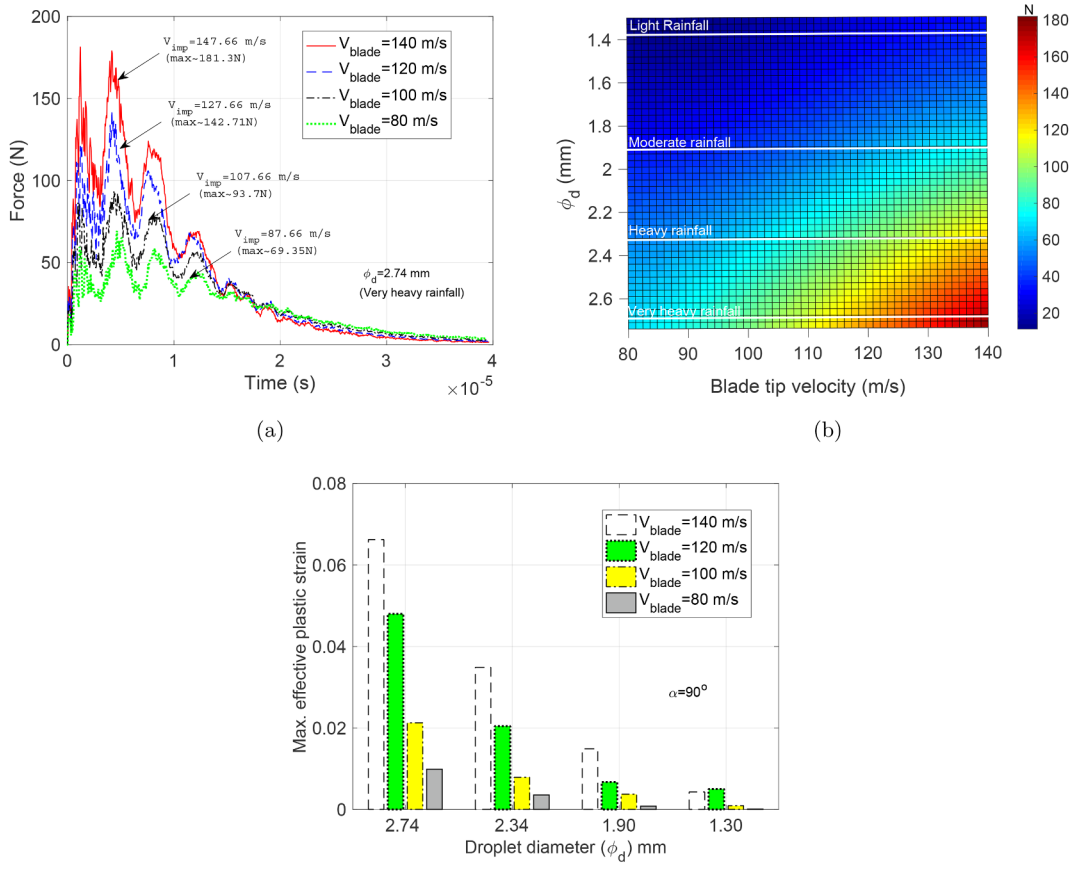

Fig. 22. (a) Comparison of contact force history for rain droplet impact for ϕ_d = 2.74 mm, α = 90° and V_{blade} = 80, 100, 120, 140 m/s (b) 2D response surface for maximum contact forces and related to rain droplet erosive variables: ϕ_d and V_{blade} (c) Comparison of maximum effective plastic strain for different ϕ_d = 2.74 mm, 2.34 mm, 1.90 mm, 1.30 mm and V_{blade} = 80, 100, 120, 140 m/s at α = 90°.

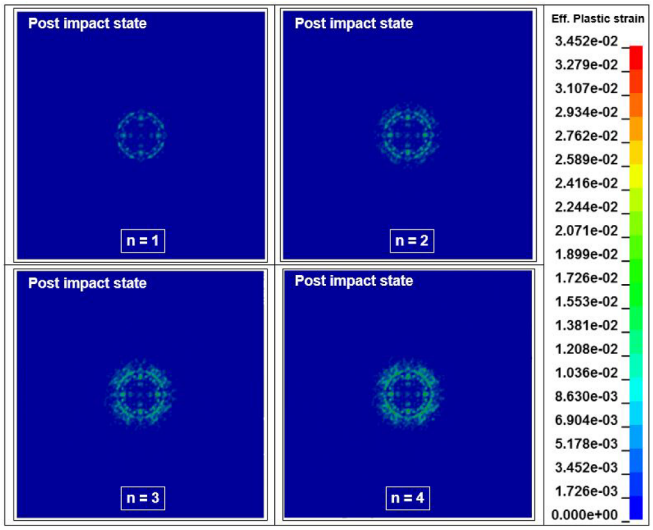

Fig. 23. Effective plastic strain for four (n = 4) repetitive rain droplet impact on the leading edge coating system for ϕ_d = 2.74 mm, α = 90° and V_{blade} = 100 m/s.

($\epsilon = 0.004466n + 0.1693$) and has $R^2 = 0.99$. Similar regression procedure is considered for impact of the leading edge coating system for different blade tip velocities (V_{blade} = 80, 120, 140 m/s) and the linear regression model is found fit to relate ϵ with n for all the cases. Fig. 24(c) presents the comparison between number of impacts required for erosion damage for different blade tip velocities. The regression curves representing different blade tip velocities are extrapolated and white dot in the figure corresponds to the number of impacts for onset of erosion damages corresponding to different blade tip velocities. The number of impacts for erosion damage increases with reducing blade tip velocity; for instance, number of impact for erosion damage is close to 150 for tip speed of 80 m/s, which reduces to around 20 for tip speed of 140 m/s. These results clearly demonstrate the merit of reducing tip speed of the blade during very heavy rainfall condition as it can significantly increase the lifetime of leading edge coating systems. Note that the utilised values used in this analysis correspond to the most critical cases of rainfall conditions together with impact at the same location and at normal impingements. In reality, these results are conservative estimates, and the number of impact for erosion onset may increase.

6. Conclusions

1. The present paper develops a coupled fluid structure interaction (FSI) computational model for simulating rain droplet impact on the wind turbine blade. The numerical model consists of structure domain modelled using traditional finite element method (FEM) whereas the fluid domain modelled using meshless method based smooth particle hydrodynamics (SPH). A particle to surface based penalty contact algorithm based on soft constraint approach is defined between the rain droplet and solid structure. A 3D numerical model is developed in LS-DYNA where the results are validated with published experimental results from the literature. Contact forces,

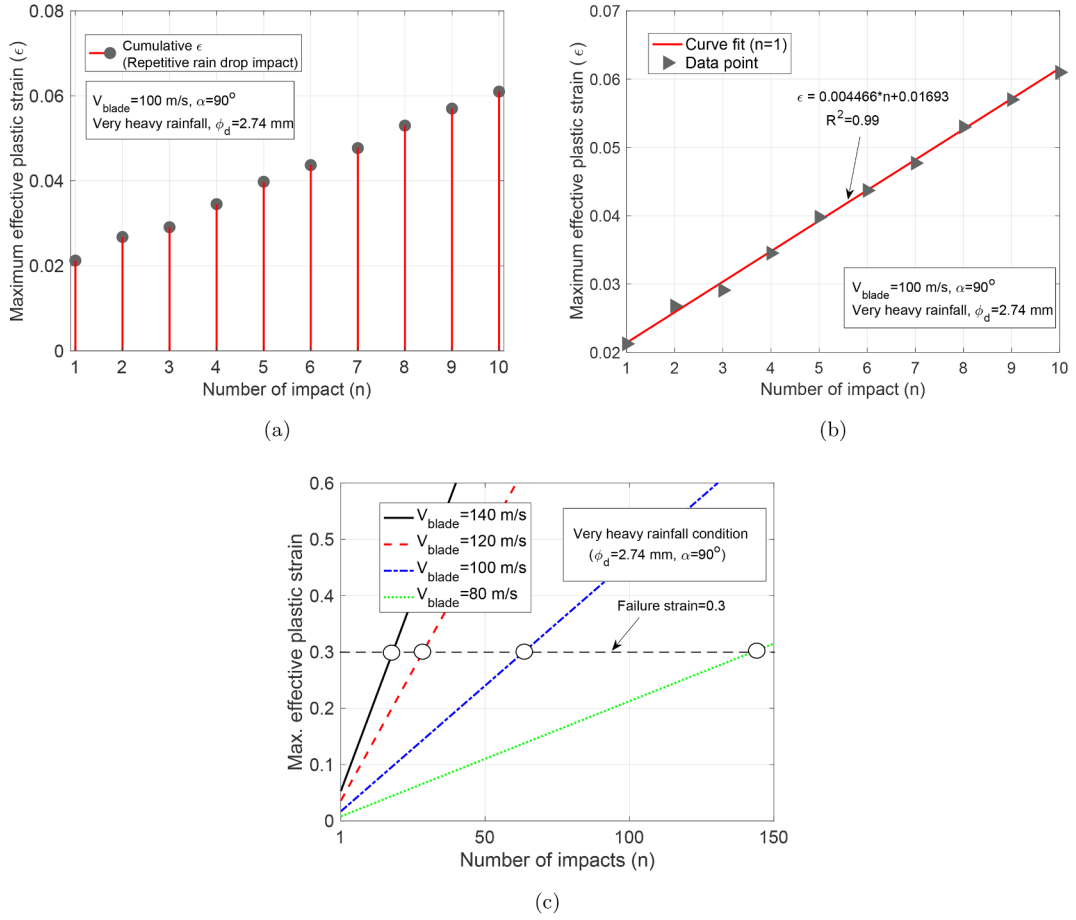

Fig. 24. (a) Cumulative effective plastic strain for ten (n = 10) repetitive rain droplet impact on the leading edge coating system (b) linear fit between ϵ and n (for ϕ_d = 2.74 mm, α = 90° and V_{blade} = 100 m/s) (c) comparison of number of impact for onset of erosion damages at the leading edge coating system for different blade tip speeds (ϕ_d = 2.74 mm, α = 90°, V_{blade} = 80, 100, 120, 140 m/s).

impulses and droplet morphology are found in good agreement.

2. A parametric study is considered to understand the effects of varying droplet size, impact angles and impact velocities on the impact responses of the leading edge coating system subjected to different rainfall conditions. Droplet sizes and droplet impact velocities considered for the analysis represent four different rainfall intensities - light rainfall (2 mm/hr), moderate rainfall (10 mm/hr), heavy rainfall (25 mm/hr), and very heavy rainfall (50 mm/hr) conditions. Detailed impact responses are described through contact forces history, droplet morphology and surface stresses developed in the leading edge coating system due to single droplet impact.
3. The contact force history is categorised into two distinct stages where active energy transfer phase includes water hammer phase and subsequent lateral jetting. This stage transmits maximum loads from the rain droplet onto the coating system and is found to have major contribution to erosion.
4. The results also show that the impact responses on the coating system increases with increasing droplet size and droplet impact angle, with maximum impulses, stresses and damages developed for normal impingement (90°). Response surface method is used to relate impulses with erosive variables: droplet size and droplet impact angle. Inclined impact angles (50° − 90°) are found as crucial erosive variables for rain erosion analysis, especially dealing with very heavy rainfall conditions (I > 25 mm/hr).
5. Ten repetitive rain droplet impacts are considered on the leading edge coating system at the same location, and maximum effective plastic strain (ϵ) is related with the number of impacts (n) using linear regression model. Finally, number of impacts to the onset of erosion damages are predicted by extrapolating the regression curve to a value corresponding to the failure strain of the gelcoat material. The number of impacts for onset of erosion damage increases with reducing blade tip velocity thereby demonstrating the merit of reducing tip speed during very heavy rainfall conditions.

7. Limitations and future work

The present study for repeated rain droplet impact is limited to a case where a single rain droplet impacts the leading edge coating system repetitively at the same location. A stochastic distribution of rain drops at the leading edge coating surface needs to be considered in the future for more realistic assessment of number of impacts required for onset of erosion damages. Also, during the repetitive rain droplet impact, relaxation of samples are not considered. Further, the main goal of the repeated rain droplet impact analysis was to compare the number of impacts required for initiation of erosion damages for different blade tip velocities. The objective was to quantify the efficiency of controlling LEE in case the rotor speed is reduced. This information is vital for developing control algorithm for reducing tip speed of the blade during harsh precipitation. To achieve this, we utilised a method already used in the literature [12] for rain droplet impact on the gelcoat-based coating system (and is valid only for such coatings where damages are dominated on the surfaces). The novelty of the method, however, is an automated script that did the work of repetitive impact compared to the literature [12] where multiple raindrops were stacked on top of each other for analysis (which is computationally demanding for an explicit solver). Nevertheless, a sound validation is essential to predict such

parameters for different coating systems, and will be performed in the future work.

In the current study, an epoxy-based thermosetting polymeric resin Epon E862 was used which does not exhibit substantially the viscoelastic behaviour, and therefore these characteristics were not included in the material modelling. These aspects would need to be considered in the future especially while dealing with flexible polyurethane coating which exhibits viscoelastic behaviour. The current paper considers coupled FSI interaction problem where the structural domain representing the wind turbine blade is modelled using conventional finite element methods, whereas the fluid domain is modelled using SPH. The developed numerical model allows a direct fluid structure interaction (FSI) coupling by simultaneously solving the displacement evolution of the SPH particles and FE nodes, whereby load transfer between both domains is attained via a penalty contact algorithm. However, other prominent computational modelling techniques should also be investigated in the future and compared with existing model. For instance., Arbitrary Lagrangian Eulerian (ALE) method has showed good correlation for impact of structures with water [49,50]; as well as meshless methods such as the material point method (MPM), which has been proven to perform more efficiently than SPH in some cases [51].'.

Data Availability

The raw/processed data required to reproduce these findings cannot be shared at this time as the data also forms part of an ongoing study.

Declaration of Competing Interest

The authors declare that they have no known competing financial interests or personal relationships that could have appeared to influence the work reported in this paper.

Acknowledgment

This work was made possible through the WINDCORE project having subsidy scheme TSE-18-04-01-Renewable energy project with project number TEHE1180113. Authors highly appreciate the financial support. The authors also appreciate anonymous reviewers for their kind comments which helped us to improve the quality of our work.

References

[1] Acero WIG. Assessment of marine operations for offshore wind turbine installation with emphasis on response-based operational limits PhD Thesis Trondheim: Norwegian University of Science and Technology (NTNU); 2016.
[2] Verma AS, Jiang Z, Vedvik NP, Gao Z, Ren Z. Impact assessment of a wind turbine blade root during an offshore mating process. Eng Struct 2019;180:205–22.
[3] Verma AS, Vedvik NP, Gao Z. A comprehensive numerical investigation of the impact behaviour of an offshore wind turbine blade due to impact loads during installation. Ocean Eng 2019;172:127–45.
[4] Pugh K, Rasool G, Stack MM. Raindrop erosion of composite materials: some views on the effect of bending stress on erosion mechanisms. J Bio-and Tribo-Corrosion 2019;5(2):45.
[5] https://www.greentechmedia.com/articles/read/an-illustrated-guide-to-the-growing-size-of-windturbines, Picture.
[6] Macdonald H, Infield D, Nash DH, Stack MM. Mapping hail meteorological observations for prediction of erosion in wind turbines. Wind Energy 2016;19(4):777–84.
[7] Bartolomé L, Teuwen J. Prospective challenges in the experimentation of the rain erosion on the leading edge of wind turbine blades. Wind Energy 2019;22(1):140–51.
[8] Keegan MH, Nash D, Stack M. On erosion issues associated with the leading edge of wind turbine blades. J Phys D: Appl Phys 2013;46(38):383001.
[9] Slot H, Gelinck E, Rentrop C, Van Der Heide E. Leading edge erosion of coated wind turbine blades: review of coating life models. Renewable Energy 2015;80:837–48.
[10] Slot H, IJzerman R, Le Feber M, Nord-Varhaug K, van der Heide E. Rain erosion resistance of injection moulded and compression moulded polybutylene terephthalate pbt. Wear 2018;414:234–42.
[11] Han W, Kim J, Kim B. Effects of contamination and erosion at the leading edge of blade tip airfoils on the annual energy production of wind turbines. Renewable energy 2018;115:817–23.
[12] Keegan MH, Nash D, Stack M. Wind turbine blade leading edge erosion: An investigation of rain droplet and hailstone impact induced damage mechanisms Ph.D. thesis University of Strathclyde; 2014.
[13] Mishnaevsky L Jr, Sütterlin , Micromechanical model of surface erosion of polyurethane coatings on wind turbine blades, Polymer Degradation and Stability.
[14] Mishnaevsky L Jr, Toolbox for optimizing anti-erosion protective coatings of wind turbine blades: Overview of mechanisms and technical solutions, Wind Energy.
[15] Mishnaevsky L Jr, Repair of wind turbine blades: Review of methods and related computational mechanics problems, Renewable energy.
[16] https://www.armouredge.com/leading-edge erosion, Picture taken.
[17] Cortés E, Sánchez F, O'Carroll A, Madramany B, Hardiman M, Young T. On the material characterisation of wind turbine blade coatings: the effect of interphase coating–laminate adhesion on rain erosion performance. Materials 2017;10(10):1146.
[18] https://www.3m.com, Picture.
[19] Cortés E, Sánchez F, Domenech L, Olivares A, Young T, O'Carroll A, Chinesta F. Manufacturing issues which affect coating erosion performance in wind turbine blades. AIP Conference Proceedings, vol. 1896. AIP Publishing; 2017. p. 030023.
[20] Bech JI, Hasager CB, Bak C, Extending the life of wind turbine blade leading edges by reducing the tip speed during extreme precipitation events, Wind Energ. Sci. Discuss.
[21] Chen J, Wang J, Ni A. A review on rain erosion protection of wind turbine blades. J Coatings Technol Res 2019;16(1):15–24.
[22] Keegan MH, Nash D, Stack M, Modelling rain drop impact on offshore wind turbine blades, ASME Turbo Expo 2012; 2012. Article-GT.
[23] Astrid B. Investigation of droplet erosion for offshore wind turbine blades. Ann Acad Med Stetin 2014;59(1):170–1.
[24] Castorrini A, Corsini A, Rispoli F, Venturini P, Takizawa K, Tezduyar TE. Computational analysis of wind-turbine blade rain erosion. Computers Fluids 2016;141:175–83.
[25] Corsini A, Castorrini A, Morei E, Rispoli F, Sciulli F, Venturini P, Modeling of rain drop erosion in a multi-mw wind turbine, ASME Paper No. GT2015-42174.
[26] Fraisse A, Bech JI, Borum KK, Fedorov V, Johansen NF-J, McGugan M, Mishnaevsky Jr L, Kusano Y. Impact fatigue damage of coated glass fibre reinforced polymer laminate. Renewable Energy 2018;126:1102–12.
[27] Zhang S, Kiil S, Dam-Johansen K, Bernad PL. Accelerated rain erosion of wind turbine blade coatings. Danmarks Tekniske Universitet (DTU) 2014.
[28] Springer GS, Erosion by liquid impact.
[29] Amirzadeh B, Louhghalam A, Raessi M, Tootkaboni M. A computational framework for the analysis of rain-induced erosion in wind turbine blades, part i: stochastic rain texture model and drop impact simulations. J Wind Eng Ind Aerodyn 2017;163:33–43.
[30] Amirzadeh B, Louhghalam A, Raessi M, Tootkaboni M. A computational framework for the analysis of rain-induced erosion in wind turbine blades, part ii: drop impact-induced stresses and blade coating fatigue life. J Wind Eng Ind Aerodyn 2017;163:44–54.
[31] Verma AS, Vedvik NP, Haselbach PU, Gao Z, Jiang Z. Comparison of numerical modelling techniques for impact investigation on a wind turbine blade. Compos Struct 2019;209:856–78.
[32] Abrate S. Impact on composite structures. Cambridge University Press; 2005.
[33] DNV G, As: Dnvgl-st-0376–rotor blades for wind turbines; 2015.
[34] Ouachan I, Kuball M, Liu D, Dyer K, Ward C, Hamerton I. Understanding of leading-edge protection performance using nano-silicates for modification. Journal of Physics: Conference Series, vol. 1222. IOP Publishing; 2019. p. 012016.
[35] Hedayati R, Ziaei-Rad S. Effect of bird geometry and orientation on bird-target impact analysis using sph method. Int J Crashworthiness 2012;17(4):445–59.
[36] Hedayati R, Sadighi M. Bird strike: an experimental, theoretical and numerical investigation. Woodhead Publishing; 2015.
[37] Monaghan JJ. Smoothed particle hydrodynamics. Ann Rev Astronomy Astrophys 1992;30(1):543–74.
[38] L.-D.K.U. Manual, I. Volume, Version 971, Livermore Software Technology Corporation 7374 (2007) 354.
[39] Zhang R, Zhang B, Lv Q, Li J, Guo P. Effects of droplet shape on impact force of low-speed droplets colliding with solid surface. Exp Fluids 2019;60(4):64.
[40] Eisenberg D, Laustsen S, Stege J. Wind turbine blade coating leading edge rain erosion model: development and validation. Wind Energy 2018;21(10):942–51.
[41] Best A. The size distribution of raindrops. Q J R Meteorol Soc 1950;76(327):16–36.
[42] Littell JD, Ruggeri CR, Goldberg RK, Roberts GD, Arnold WA, Binienda WK. Measurement of epoxy resin tension, compression, and shear stress–strain curves over a wide range of strain rates using small test specimens. J Aerospace Eng 2008;21(3):162–73.
[43] A. International, ASTM D638-14, Standard Test Method for Tensile Properties of Plastics, ASTM International, 2015.
[44] Ramakrishnan KR. Low velocity impact behaviour of unreinforced bi-layer plastic laminates. University of New South Wales, Australian Defence Force Academy; 2009.
[45] Perillo G, Vedivik N, Echtermeyer A. Damage development in stitch bonded GFRP composite plates under low velocity impact: Experimental and numerical results. J Compos Mater 2015;49(5):601–15.
[46] Zhang B, Li J, Guo P, Lv Q. Experimental studies on the effect of reynolds and weber numbers on the impact forces of low-speed droplets colliding with a solid surface. Exp Fluids 2017;58(9):125.
[47] Zhang B, Lv Q, Guo P, Li J. Experimental study of impact force of a low-speed droplet colliding on the solid surface at different impact angles. ASME 2017 International Mechanical Engineering Congress and Exposition. American Society of Mechanical Engineers Digital Collection; 2017.

[48] Gohardani O. Impact of erosion testing aspects on current and future flight conditions. Progress Aerospace Sci 2011;47(4):280–303.
[49] Hua C, Fang C, Cheng J. Simulation of Fluid-Solid Interaction on Water Ditching of an Airplane by Ale Method. J Hydrodyn 2011;23(5):637–42. https://doi.org/10.1016/S1001-6058(10)60159-X.
[50] Bisagni C, Pigazzini M. Modelling strategies for numerical simulation of aircraft ditching. Int J Crashworthiness 2018;23(4):377–94. https://doi.org/10.1080/13588265.2017.1328957.
[51] He L, Huang Z, Liu H, Li H, Gan Y, Sun Z. Material point method and smoothed particle hydrodynamics simulations of fluid flow problems: a comparative study. Progress Comput Fluid Dyn Int J 2018;18(1):1. https://doi.org/10.1504/PCFD.2016.10001222.